Quantitative Finance

ISSN: 1469-7688 (Print) 1469-7696 (Online) Journal homepage: http://www.tandfonline.com/loi/rquf20

Estimation of risk-neutral measures using quartic B-spline cumulative distribution functions with power tails

Seung Hwan Lee

To cite this article: Seung Hwan Lee (2014) Estimation of risk-neutral measures using quartic B-spline cumulative distribution functions with power tails, Quantitative Finance, 14:10, 1857-1879, DOI: 10.1080/14697688.2012.742202

To link to this article: https://doi.org/10.1080/14697688.2012.742202

Quantitative Finance, 2014
Vol. 14, No. 10, 1857–1879, http://dx.doi.org/10.1080/14697688.2012.742202

Routledge
Taylor & Francis Group

Estimation of risk-neutral measures using quartic B-spline cumulative distribution functions with power tails

SEUNG HWAN LEE*

The Bank of Korea, 110, 3-Ga, Namdaemun-Ro, Jung-Gu, Seoul 100-794, Republic of Korea

(*Received 2 November 2009; in final form 17 October 2012*)

In this paper, we propose the B-spline (BSP) method, which overcomes problems with the smoothed implied volatility smile (SML) method for estimating option implied risk-neutral measures (RNMs). We model the risk-neutral cumulative distribution function (CDF) using quartic B-splines with power tails so that the resulting risk-neutral probability density function (PDF) has continuity C^2 and arbitrage-free properties. Since the number of knots is selected optimally in constructing the quartic B-spline risk-neutral CDF, our method avoids both overfitting and oversmoothing. To improve computational efficiency and accuracy, we introduce a three-step RNM estimation procedure that transforms a nonlinear optimization problem into a convex quadratic program. Monte-Carlo experiments and applications to S&P 500 index options suggest that the BSP method performs considerably better than the SML method. The BSP method always produces arbitrage-free RNM estimators and almost perfectly recovers the actual risk-neutral PDFs for various hypothetical distributions.

Keywords: Risk neutral distribution; Numerical method; Option pricing; Optimization

JEL Classification: C1, C14, G1, G13

1. Introduction

Investors and researchers have long used option prices to infer market expectations about the volatilities and correlations of the underlying assets by recovering risk-neutral distributions from the observed option prices. Option prices are computed as a present value of its expected payoffs under the risk-neutral (probability) measure (RNM). The RNM can be estimated from a set of European option prices using the relationship proposed by Ross (1976) and Breeden and Litzenberger (1978). Since the RNM embodies important information about market participants' sentiments concerning prices of the underlying asset in the future, a number of methods have been developed to estimate the RNM from the observed option prices. Generally, these methods are divided into the two broad groups of parametric and non-parametric methods.†

The parametric methods make particular assumptions on the form or family of the RNM and then typically use a nonlinear regression technique to estimate the parameters of the RNM that minimizes the sum of squared pricing errors. On the other hand, the non-parametric methods make no strong assumptions about the RNM since they are flexible data-driven methods. However, the non-parametric approaches are so data-intensive that they usually lead to over-fitting problems and are not effective for small samples.

The most widely used non-parametric technique for estimating RNMs is the smoothed implied volatility smile (SML) method, which has been discerned as a standard method by users such as central banks and market participants. The SML method was originally developed by Shimko (1993), and it explicitly utilizes the results of Breeden and Litzenberger (1978) on the call option pricing function. Shimko (1993) proposes that the observed option prices first be converted to implied volatilities using the Black–Scholes option pricing formula. A continuous smoothing function is then fitted to implied volatilities against the strike prices. The implied volatility function can then be fitted and the continuum of fitted implied volatilities converted back into a continuum of fitted option prices.

*Email: leecon@bok.or.kr

†The term non-parametric is not meant to imply that such models completely lack parameters, but that the number and nature of the parameters are flexible and not fixed in advance.

The RNM probability density function (PDF) can be obtained by applying the results of Breeden and Litzenberger (1978) on the call option pricing function. The advantage of this method is that the implied volatilities are much more similar in magnitude across strike prices than are option prices. Bliss and Panigirtzoglou (2002) follow Malz (1997) in smoothing in implied volatility/delta space and Campa *et al.* (1998) in using a natural cubic spline to approximate the function. Recently, Bu and Hadry (2007) improved the SML method by providing an analytic expression for the RNM estimator.

The SML method has some problems in estimating the RNM. First, the natural spline is restricted to become linear outside the range of observed option prices. As Bliss and Panigirtzoglou (2002) point out, this restriction can lead to negative tail probabilities if the slope of the polynomial is negative at the extreme knot points.† Further, the estimated tail probabilities contain no information about the true probabilities since they are not estimated by observed option prices. Second, the SML method cannot guarantee the resulting risk-neutral PDF to be integrated to unity. The negative probabilities or probabilities not integrating to unity seriously violate no-arbitrage constraints. Lastly, problems with the SML method include the difficulty of selecting the optimal tradeoff between smoothness and fit since the shape of risk-neutral PDFs is very sensitive to the smoothing parameter. The SML method is unable to avoid both overfitting and oversmoothing. To effectively eliminate noise in the data, this method requires substantial smoothing, which considerably distorts the genuine features of the estimated function.

This paper proposes a new approach that overcomes the drawbacks of the SML method. First, we model the probability distribution outside the traded strike range as power tails, which may be estimated from the far-from-the-money option prices. With the power tails, the RNM has non-negative tail probabilities and also reflects information about the true tail probabilities. Second, the RNM cumulative distribution function (CDF) is constructed by using quartic B-spline functions with power tails so that the resulting risk-neutral PDF has continuity C^2. The use of B-splines also improves computational efficiency and reduces the number of spline parameters since every spline function can be represented as a linear combination of B-splines. The advantage of constructing the risk-neutral CDF with power tails is that the sum of RNM probabilities is guaranteed to be unity. Lastly, by choosing the optimum number of knots, our method can avoid both overfitting and oversmoothing. A small number of knots may result in a function space that is not flexible enough to capture the true risk-neutral CDF but, on the other hand, a large number may lead to serious overfitting. To select an optimal tradeoff between smoothness and fit, we use the minimum number of knots that attains zero bid–ask pricing errors. The method is termed the B-spline risk-neutral CDF with power tails (BSP).‡

The BSP method involves solving a highly nonlinear optimization problem with a number of constraints due to the power tails. It is computationally difficult and inaccurate to estimate the B-spline part of the CDF and the power tails simultaneously. To improve computational efficiency and accuracy, we develop a three-step RNM estimation technique: (i) estimating the power tail parameters; (ii) selecting the optimum number of knots; and (iii) estimating the B-spline control points. The three-step estimation procedure transforms a nonlinear optimization problem into a convex quadratic program that is efficiently solved by numerical optimization software.

To compare the performance of the BSP method with the SML method for estimating option implied RNMs, we evaluate the two methods on the basis of the flexibility of the estimated RNM and conduct Monte-Carlo experiments based on 12 hypothetical true distributions. We find that the BSP method dominates the SML method as a technique for estimating option implied RNM. The SML method violates the no-arbitrage constraints, and it is significantly biased, particularly under scenarios where the true RNM is a fat-tailed distribution. In contrast, the BSP method always produces arbitrage-free RNM estimators, and it almost perfectly recovers the actual risk-neutral PDFs for all hypothetical distributions. Further, in order to address the robustness of the RNM estimation methods, we apply the two methods to the S&P 500 index option market data. Our application to real market data confirms the Monte-Carlo simulation results.

The rest of the paper is organized as follows. Section 2 briefly reviews the smoothed implied volatility smile (SML) method. Section 3 derives option pricing functions based on the quartic B-spline risk-neutral CDF with power tails. Section 4 introduces the three-step RNM estimation procedure for the quartic B-spline risk-neutral CDF with power tails. In section 5, we compare the flexibility of the BSP method and SML method by Monte-Carlo experiments and applications to real market data. Section 6 concludes.

2. Smoothed implied volatility smile (SML) method

The smoothed implied volatility smile method explicitly utilizes the results of Breeden and Litzenberger (1978) on the call option pricing function. Breeden and Litzenberger showed that the risk-neutral PDF of the price of the underlying asset at maturity is related to call (or put) prices through

$$R'(S_T) = e^{rT} \left. \frac{\partial^2 C(K)}{\partial K^2} \right|_{K=S_T},$$

†The linearity of the SLM method outside the range of observed strike prices does not imply a flat extrapolation scheme. The SML method extrapolates outside the range of available data with second-order smoothness conditions as in Jiang and Tian (2007). Jiang and Tian (2007) improve the flat extrapolation scheme of Jiang and Tian (2005) and Carr and Wu (2009), which satisfies first-order smoothness, resulting in the implied volatility function being flat beyond listed strike prices.

‡The B-spline CDF with power tails has infinite-dimensional control points since the number of knots is not fixed in advance. However, it also has finite-dimensional tail parameters and thus it is not a pure non-parametric method. A model is called semi-non-parametric if it has both finite-dimensional and infinite-dimensional unknown parameters of interest.

where $R(\cdot)$ is the risk-neutral CDF, S_T is the underlying asset price at maturity, r is the risk-free interest rate, T is the time to maturity, K is the strike price, and $C(K)$ is the call pricing function. Thus, if we observed the call pricing function we could differentiate twice to obtain the risk-neutral PDF. However, we only observe option prices for relatively few discretely spaced strikes.

Shimko (1993) proposes interpolating in the implied volatility domain instead of the call price domain since it is technically difficult to fit accurately the shape of the latter and small fitted price errors tend to have large effects on the resulting risk-neutral PDFs, particularly in the tails. Shimko (1993) chose to use a simple quadratic polynomial smoothing function within the span of available strikes and with log-normal tails outside the span of available strikes. Malz (1997) modified Shimko's technique by fitting the implied volatility against the Black–Scholes option delta ($\delta = \partial C/\partial S$) rather than strike price, but follows Shimko in using a low-order polynomial as the smoothing function. Campa *et al.* (1998) introduced the use of a smoothing spline† for fitting implied volatility curves. They apply this to smoothing the implied volatility/strike function. Use of a natural spline, rather than a low-order polynomial, permits the user to control the smoothness of the fitted function.

In this paper, we use the smoothed implied volatility smile (SML) method developed by Bliss and Panigirtzoglou (2002). This method follows Malz (1997) in smoothing in implied volatility/delta space and Campa *et al.* (1998) in using a smoothing cubic spline to approximate the function. The risk-neutral PDF can be obtained using a five-step estimation procedure.

- **Step 1:** Converting call option prices, C_{K_i}, into implied volatilities, σ_{K_i}, using the inverse Black–Scholes formula‡

$$\sigma_{K_i} = BS^{-1}(C_{K_i}, K_i, S_0, r, d, T),$$

where $BS^{-1}(\cdot)$ is the inverse Black–Scholes formula, σ_{K_i} and C_{K_i} are the implied volatility and the price of a European call option, respectively, associated with the strike price K_i, S_0 is the underlying asset price at time 0, r is the risk-free rate, d is the dividend rate, and T is the maturity date.

- **Step 2:** Converting implied volatility/strike space into implied volatility/delta space

$$\delta_i = e^{-dT}\Phi\left(\frac{\ln S_0 - \ln K_i + (r - d + \sigma_A^2/2)T}{\sigma_A\sqrt{T}}\right),$$
$$IV(\delta_i) = \sigma_{K_i},$$

where δ_i is the delta associated with the strike price K_i§; σ_A is the at-the-money volatility,¶ $IV(\delta_i)$ is the implied volatility associated with δ_i, and $\Phi(\cdot)$ is the standard normal CDF. Since σ_{K_i} is the implied volatility associated with K_i, which corresponds to δ_i, the implied volatility associated with δ_i should be the same as σ_{K_i}.

- **Step 3:** Approximating the implied volatility smile using smoothing cubic spline functions

$$\min_{\Theta} \sum_{i=1}^{N} w_i(IV(\delta_i) - f(\delta_i;\Theta))^2 + \omega\int_0^{e^{-dT}} f''(\delta;\Theta)^2 \mathrm{d}\delta,$$

where Θ is the matrix of spline parameters of the cubic spline, $f(\cdot;\Theta)$ is the cubic spline function given the spline parameters Θ, $f(\delta_i,\Theta)$ is the fitted implied volatility at δ_i, w_i is the relative weights to each observation,|| and ω is the smoothing parameter, which multiplies a measure of the degree of curvature in the function—the integral of the squared second derivative of the function over its range.††

- **Step 4:** Converting the implied volatility smile into an option pricing function in price/strike space

$$\delta(K) = e^{-dT}\Phi\left(\frac{\ln S_0 - \ln K + (r - d + \sigma_A^2/2)T}{\sigma_A\sqrt{T}}\right),$$
$$\sigma(K) = f(\delta(K);\Theta),$$
$$C(K) = BS(K, \sigma(K), S_0, r, d, T),$$

where $\sigma(K)$ is the fitted implied volatility smile, $C(K)$ is the fitted call pricing function, and $BS(\cdot)$ is the Black–Scholes formula.

- **Step 5:** Computing the risk-neutral PDF using numerical methods

†The curve fitting method based on spline functions was first used by McCulloch (1971, 1975) in finance for modeling the term structure of interest rates.

‡The use of the Black–Scholes formula to transfer between the call price and implied volatility domains does not require that the Black–Scholes model is true. The Black–Scholes formula is used as a translation device that allows us to interpolate implied volatilities rather than the observed option prices themselves for computational convenience.

§It should be recalled that $0 \leq \delta_i \leq e^{-dT}$, where d is the dividend rate of the underlying asset.

¶Transforming each strike into a delta using the at-the-money implied volatility has the advantage that the ordering of deltas is always the same as that of the strikes. Panigirtzoglou and Skiadopoulos (2004) pointed out that using the implied volatilities that corresponds to each strike could change the ordering in the delta space, in cases where steep volatility skews are observed. This would result in generating volatility smiles with artificially created kinks.

||Bliss and Panigirtzoglou (2002) discussed different types of weighting schemes and how the weighting can account for different sources of pricing errors.

††The objective function suggests that the degree of freedom for the estimation is also related to the smoothing parameter. In particular, the maximum degree of freedom is achieved when $\omega = 1$, which amounts to fitting a straight line to the data, whereas when $\omega = 0$, the cubic spline provides an exact fit to the data. Fisher *et al.* (1995) give a rigorous definition of the effective number of parameters of the regression.

$$R'(x) = e^{rT}\frac{\partial^2 C(x)}{\partial x^2},$$

where $R'(x)$ is the risk-neutral PDF.

3. Quartic B-spline risk-neutral CDF with power tails

3.1. Uniform quartic B-spline

A spline is a piecewise polynomial function. A spline $S : [a,b] \to R$ consists of polynomial pieces $P_i : [x_i, x_{i+1}) \to R$, where

$$a = x_1 < \cdots < x_n = b.$$

The given n points x_i are called knots. The vector $x = (x_1, \ldots, x_n)$ is called the knot vector for the spline. A spline on $[a,b]$ is of degree m if its first $m-1$ derivatives exist on each interior knot and the highest degree of the polynomials defining the spline function is m.

A B-spline is the spline function that has minimal support with respect to given order, smoothness, and domain partitions. Every spline function of given degree, smoothness and domain partition can be represented as a linear combination of B-splines of the same order and smoothness, and over that same partition. A B-spline basis function of degree m is the piecewise polynomial whose pieces are defined over the spans between knots. Each piece is a polynomial of degree m. The pieces meet with continuity of all derivatives below the mth and with (possible) discontinuities of the mth derivative. The function is identically zero outside a range of $m+1$ spans, and positive within its non-zero domain.

The ith B-spline basis of degree m for n knots x_i with $x_1 < x_2 < \cdots < x_n$ can be constructed using the Cox–de Boor recursion formula:

$$B_{i,0}(x) = I_{[x_i, x_{i+1})}(x), \tag{1}$$

$$B_{i,m}(x) = \frac{x - x_i}{x_{i+m} - x_i}B_{i,m-1}(x) + \frac{x_{i+m+1} - x}{x_{i+m+1} - x_{i+1}}B_{i+1,m-1}(x), \tag{2}$$

where $I_{[x_i, x_{i+1})}(x) = 1$ for $x \in [x_i, x_{i+1})$, $I_{[x_i, x_{i+1})}(x) = 0$ for $x \notin [x_i, x_{i+1})$, $B_{i,m}(x) > 0$ for $x \in [x_i, x_{i+m+1}]$, and $B_{i,m}(x) = 0$ for $x \notin [x_i, x_{i+m+1}]$. When the knots are equidistant, we say the B-spline is uniform, otherwise we call it non-uniform. In this paper, we use the uniform quartic B-spline basis to construct the risk-neutral CDF.

A quartic spline is the spline of degree 4 with C^3 continuity. The quartic spline can be constructed as a linear combination of fourth degree B-spline basis functions:

$$f(x) = \sum_{i=1}^{n-5} c_i B_{i,4}(x), \quad x \in [x_5, x_{n-4}].$$

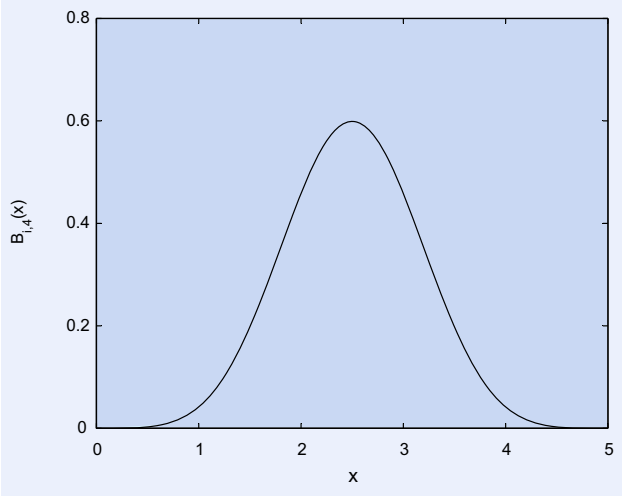

Figure 1. The uniform quartic B-spline basis function, where $x_i = 0$ and $\Delta x = 1$.

The coefficients c_i are called the control points.† The uniform quartic B-spline basis function is illustrated in Figure 1.

Consider a uniform knot vector $x = (x_1, \ldots, x_n)$ with $(x_{i+1} - x_i) = h$ for all $i = 1, \ldots, n-1$. Since knots are equidistant,

$$\frac{x_{i+j} - x_i}{h} = j. \tag{3}$$

In order to simplify notation, let

$$z_i \equiv \frac{x - x_i}{h}, \tag{4}$$

$$z_{i+j} \equiv \frac{x - x_{i+j}}{h}. \tag{5}$$

By combining (3) and (5),

$$z_{i+j} = z_i - j. \tag{6}$$

By means of (4) and (6), we can rewrite the Cox–de Boor formula (1) and (2):

$$B_{i,0}(x) = I_{[x_i, x_{i+1})}(x), \tag{7}$$

$$B_{i,m}(x) = \frac{z_i}{m}B_{i,m-1}(x) + \frac{m + 1 - z_i}{m}B_{i+1,m-1}(x). \tag{8}$$

Finally, we may construct the basis of a uniform quartic B-spline recursively by using (7) and (8):

†The control points form a sequence that is known as the control polygon which is often visualized by joining them in sequence by straight lines. This set of straight lines is in fact the B-spline curve of order 1 defined by that set of control points. For more details, see de Boor (1978).

$$
\begin{aligned}
B_{i,4}(x) = &\left(\frac{z_i^4}{24}\right) I_{[x_i,x_{i+1})}(x) \\
&+ \left(\frac{-4z_i^4 + 20z_i^3 - 30z_i^2 + 20z_i - 5}{24}\right) I_{[x_{i+1},x_{i+2})}(x) \\
&+ \left(\frac{6z_i^4 - 60z_i^3 + 210z_i^2 - 300z_i + 155}{24}\right) I_{[x_{i+2},x_{i+3})}(x) \\
&+ \left(\frac{-4z_i^4 + 60z_i^3 - 330z_i^2 + 780z_i - 655}{24}\right) I_{[x_{i+3},x_{i+4})}(x) \\
&+ \left(\frac{(5 - z_i)^4}{24}\right) I_{[x_{i+4},x_{i+5})}(x),
\end{aligned}
$$

where $z_i = (x - x_i)/h$ and $h = x_{i+1} - x_i$.

3.2. Constructing a quartic B-spline risk-neutral CDF with power tails

Consider N traded strike price sequences $K_1 < K_2 < \cdots < K_N$. We construct a risk-neutral CDF by means of the quartic B-spline for the traded strike range $[K_1, K_N]$, and then extrapolate beyond the traded strike range by grafting power tails onto each of the endpoints of the risk-neutral CDF. To ensure a smooth transition from the traded strike range of the distribution to the tails, we impose end point constraints for continuity up to the second derivative. To guarantee the non-negativity of the risk-neutral PDF, we also restrict the slope of the risk-neutral CDF to be non-negative at all the knot points within the traded strike range $[K_1, K_N]$. Thus, the quartic B-spline CDF with power tails is described as

$$
\begin{aligned}
R(x) &= R(x; c_1, \ldots, c_{n-5}, \rho_1, \rho_2, \lambda_1, \lambda_2) \\
&= \rho_1 x^{\lambda_1} I_{[0,K_1)}(x) + \sum_{i=1}^{n-5} c_i B_{i,4}(x) I_{[K_1,K_N]}(x) \\
&\quad + (1 - \rho_2 x^{-\lambda_2}) I_{(K_N,\infty]}(x),
\end{aligned} \tag{9}
$$

s.t.

(i) Level continuity constraints

$$
\rho_1 K_1^{\lambda_1} = \sum_{i=1}^{n-5} c_i B_{i,4}(K_1) \qquad \text{(left end)}, \tag{10}
$$

$$
1 - \rho_2 K_N^{-\lambda_2} = \sum_{i=1}^{n-5} c_i B_{i,4}(K_N) \qquad \text{(right end)}. \tag{11}
$$

(ii) First derivative continuity constraints

$$
\rho_1 \lambda_1 K_1^{\lambda_1 - 1} = \sum_{i=1}^{n-5} c_i B_{i,4}^{(1)}(K_1) \qquad \text{(left end)}, \tag{12}
$$

$$
\rho_2 \lambda_2 K_N^{-\lambda_2 - 1} = \sum_{i=1}^{n-5} c_i B_{i,4}^{(1)}(K_N) \qquad \text{(right end)}. \tag{13}
$$

(iii) Second derivative continuity constraints

$$
\rho_1 \lambda_1 (\lambda_1 - 1) K_1^{\lambda_1 - 2} = \sum_{i=1}^{n-5} c_i B_{i,4}^{(2)}(K_1) \qquad \text{(left end)}, \tag{14}
$$

$$
-\rho_2 \lambda_2 (\lambda_2 + 1) K_N^{-\lambda_2 - 2} = \sum_{i=1}^{n-5} c_i B_{i,4}^{(2)}(K_N) \qquad \text{(right end)}. \tag{15}
$$

(iv) Non-negative probability constraints

$$
\sum_{i=1}^{n-5} c_i B_{i,4}^{(1)}(x_j) \geq 0, \quad j = 6, \ldots, n-5, \tag{16}
$$

where $x = (x_1, \ldots, x_n)$ is a uniform knot vector with $x_5 = K_1$ and $x_{n-4} = K_N$, and $B^{(j)}$ denotes the jth derivative of the B-spline basis.

The non-negativity constraints (16) check for non-negativity of the risk-neutral probabilities only at the knots, not for all the points in the strike price domain. However, Monte-Carlo experiments and applications to S&P data show that, in most cases, the non-negativity constraint (16) is enough to produce non-negative probabilities for all the strike price domain (see table 3). Nevertheless, it is possible that slight negative probabilities occur between knot points. If negative probabilities are found, there are three ways to remedy them. Firstly, we may choose the number of knots (n) that satisfies the non-negative minimum probability condition:

$$
\min\left(\sum_{i=1}^{n-5} c_i B_{i,4}^{(1)}(x)\right) \geq 0, \quad K_1 < x < K_N.
$$

Secondly, we may impose an additional non-negativity constraint at the point around which the negative probabilities occur:

$$
\sum_{i=1}^{n-5} c_i B_{i,4}^{(1)}(x_a) \geq 0, \quad R''(x_a) < 0.
$$

Finally, we may impose positive semidefinitness constraints, which guarantee non-negativity in the entire domain, proposed by Monterio *et al.* (2008). The positive semidefiniteness constraints are convex constraints and thus the resulting problem can be reformulated as a convex semidefinite programming problem with a quadratic objective function (Monterio *et al.* 2008).†

†Monterio *et al.* (2008) estimate the cubic spline risk-neutral PDF only for the traded strike range by truncating the tails of the PDF without estimating them from observed option prices. Fengler (2009) proposed an algorithm for estimating the implied volatility smile under suitable linear inequality constraints, ensuring non-negativity of the risk-neutral PDF, but this algorithm does not guarantee the resulting risk-neutral PDF to be integrated to unity.

Once we have the quartic B-spline risk-neutral CDF with power tails, $R(x)$, the risk-neutral PDF can be derived as a first derivative of $R(x)$:

$$R'(x) = \rho_1\lambda_1 x^{\lambda_1-1} I_{[0,K_1)}(x) + \sum_{i=1}^{n-5} c_i B_{i,4}^{(1)}(x) I_{[K_1,K_N]}(x) + \rho_2\lambda_2 x^{-\lambda_2-1} I_{(K_N,\infty]}(x), \quad (17)$$

where

$$\begin{aligned} B_{i,4}^{(1)}(x) = &\left(\frac{z_i^3}{6h}\right) I_{[x_i,x_{i+1})}(x) \\ &+ \left(\frac{-4z_i^3 + 15z_i^2 - 15z_i + 5}{6h}\right) I_{[x_{i+1},x_{i+2})}(x) \\ &+ \left(\frac{6z_i^3 - 45z_i^2 + 105z_i - 75}{6h}\right) I_{[x_{i+2},x_{i+3})}(x) \\ &+ \left(\frac{-4z_i^3 + 45z_i^2 - 165z_i + 195}{6h}\right) I_{[x_{i+3},x_{i+4})}(x) \\ &+ \left(\frac{z_i^3 - 15z_i^2 + 75z_i - 125}{6h}\right) I_{[x_{i+4},x_{i+5})}(x) \end{aligned}$$

with $z_i = (x - x_i)/h$, $h = x_{i+1} - x_i$. The quartic B-spline risk-neutral CDF and PDF with power tails are illustrated in Figure 2.

Since the risk-neutral CDF is constructed using quartic B-splines, the resulting risk-neutral PDF has C^2 continuity. We construct C^2 continuous PDFs because they provide the simplest representation that exhibits the desired appearance of smoothness. Note C^2 continuity is the lowest-order spline endowed with inflection points and higher-order splines tend to exhibit the instabilities inherent in higher-order polynomials (ill-conditioning or oscillations).

3.3. Option pricing with the B-spline risk-neutral CDF

By ruling out arbitrage possibilities, Cox and Ross (1976) showed that options can be priced as if investors were risk neutral, regardless of investors' risk preferences. Consider a general European call option whose terminal payoff is $\max(0, S_T - K)$, where S_T is the underlying asset price at maturity, T is the maturity date, and K is the strike price. In a complete arbitrage-free market, the price of a European call option, $C(K)$, can then be computed as the discounted value of the option's expected payoff under the RNM. Formally,

$$\begin{aligned} C(K) &= e^{-rT}\int_K^\infty (x - K)R'(x)\mathrm{d}x \\ &= e^{-rT}\left[\int_K^\infty xR'(x)dx + KR(K) - K\right], \end{aligned} \quad (18)$$

where r is the risk-free rate, and $R'(x)$ is the risk-neutral density of the underlying asset price at maturity.

In a similar manner, the price of a European put option, $P(K)$, can be calculated as

$$P(K) = e^{-rT}\int_0^K (K - x)R'(x)\mathrm{d}x = e^{-rT}\left[-\int_0^K xR'(x)\mathrm{d}x + KR(K)\right]. \quad (19)$$

In the arbitrage-free market, the expected price at maturity under the RNM should equal the forward price of the

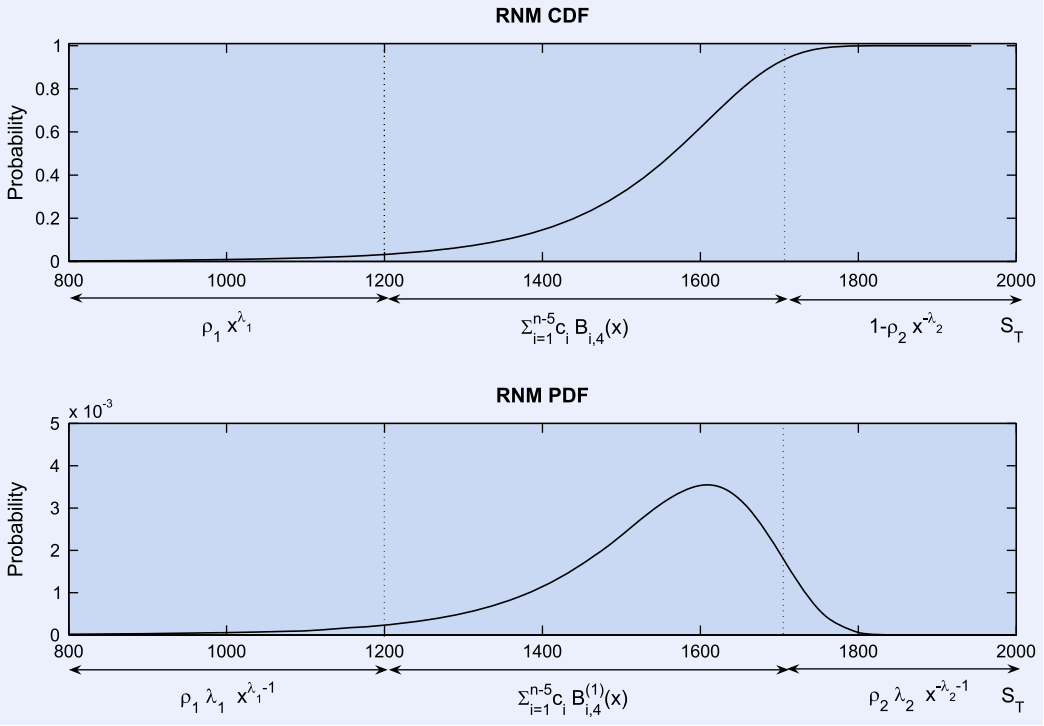

Figure 2. The quartic B-spline risk-neutral CDF and PDF with power tails.

underlying asset with the same time to maturity, i.e. the RNM must satisfy the so-called mean-forward price equality condition:

$$E^{Q}(S_T) = \int_0^{\infty} xR'(x)\mathrm{d}x = S_0 e^{(r-d)T}, \tag{20}$$

where S_t is the underlying asset price at time t, d is the annual dividend rate of the underlying asset, $S_0 e^{(r-d)T}$ is the implicit forward price, and E^{Q} is the conditional expectation on time 0 information under the RNM.

By applying the B-spline RNM (9) and (17) to call and put price functions (18) and (19), call and put option prices under the B-spline risk-neutral CDF with power tails are written as

$$\begin{aligned} C(K;\mathbf{c},\boldsymbol{\theta}) = {} & e^{-rT}\Big[\sum_{i=1}^{n-5} c_i \int_K^{K_N} xB_{i,4}^{(1)}(x)dx + \frac{\rho_1\lambda_1}{\lambda_1+1}K_1^{\lambda_1+1} \\ & + \frac{\rho_2\lambda_2}{\lambda_2-1}K_N^{-\lambda_2+1} + \frac{\rho_1}{\lambda_1+1}K^{\lambda_1+1} - K\Big]I_{[0,K_1)}(K) \\ & + e^{-rT}\Big[\sum_{i=1}^{n-5} c_i\Big(KB_{i,4}(K) + \int_K^{K_N} xB_{i,4}^{(1)}(x)dx\Big) \\ & + \frac{\rho_2\lambda_2}{\lambda_2-1}K_N^{-\lambda_2+1} - K\Big]I_{[K_1,K_N]}(K) \\ & + e^{-rT}\frac{\rho_2}{\lambda_2-1}K^{-\lambda_2+1}I_{(K_N,\infty]}(K), \end{aligned} \tag{21}$$

and

$$\begin{aligned} P(K;\mathbf{c},\boldsymbol{\theta}) = {} & e^{-rT}\frac{\rho_1}{\lambda_1+1}K^{\lambda_1+1}I_{[0,K_1)}(K) \\ & + e^{-rT}\Big[\sum_{i=1}^{n-5} c_i\Big(KB_{i,4}(K) - \int_{K_1}^{K} xB_{i,4}^{(1)}(x)dx\Big) \\ & - \frac{\rho_1\lambda_1}{\lambda_1+1}K_1^{\lambda_1+1}\Big]I_{[K_1,K_N]}(K) \\ & + e^{-rT}\Big[-\sum_{i=1}^{n-5} c_i KB_{i,4}(K) - \frac{\rho_1\lambda_1}{\lambda_1+1}K_1^{\lambda_1+1} \\ & - \frac{\rho_2\lambda_2}{\lambda_2-1}K_N^{-\lambda_2+1} + \frac{\rho_2}{\lambda_2-1}K^{-\lambda_2+1} + K\Big]I_{(K_N,\infty]}(K), \end{aligned} \tag{22}$$

where $\mathbf{c} = [c_1 \ldots c_{n-5}]'$ and $\boldsymbol{\theta} = [\rho_1\rho_2\lambda_1\lambda_2]'$. The derivation of the call and put pricing functions (21) and (22) is given in appendix A.

4. Estimation of the risk-neutral CDF

4.1. Optimization problem

Since the out-of-the-money (OTM) options are generally more liquid than the in-the-money (ITM) options, we estimate the risk-neutral CDF, $R(x)$, from each cross-section of the OTM option prices with the different strike prices K_i and the same time to maturity T. The OTM option prices are defined as

$$V(K_i) = \begin{cases} P(K_i), & K_i < F, \\ \frac{P(K_i)+C(K_i)}{2}, & K_i = F, \\ C(K_i), & K_i > F, \end{cases} \quad i = 1, \ldots, N,$$

where $P(K_i)$ and $C(K_i)$ are the traded put and call option prices, respectively, associated with strike price K_i and F is the forward price. By put–call parity, the OTM option prices can be alternatively defined as

$$V(K_i) = \min[C(K_i), P(K_i)], \quad i = 1, \ldots, N.$$

Similarly, under the quartic B-spline risk-neutral CDF with power tails, $R(x;\boldsymbol{\theta},\mathbf{c})$, the OTM option model prices are defined as

$$V(K_i;\mathbf{c},\theta) = \min[C(K_i;\mathbf{c},\boldsymbol{\theta}), P(K_i;\mathbf{c},\boldsymbol{\theta})], \quad i = 1, \ldots, N.$$

The vector of tail parameters, $\boldsymbol{\theta}$, and control points, $\boldsymbol{c}$, can be simply estimated by the least squares criterion, i.e. minimizing the sum of squared pricing errors (SSE) given the number of knots, n:

$$\min_{\mathbf{c},\boldsymbol{\theta}} L(SSE) = \sum_{i=1}^{N}(V(K_i) - V(K_i;\mathbf{c},\boldsymbol{\theta}))^2.$$

However, since the least squares criterion cannot reduce rapid local variations of the estimated risk-neutral PDF, the roughness penalty is introduced in the loss function to prevent wiggly risk-neutral PDFs. The roughness penalty for the risk-neutral PDF is defined as the integrated squared third derivative of the risk-neutral CDF:

$$\int_{K_1}^{K_N} [R'''(x;\mathbf{c},\boldsymbol{\theta})]^2 dx.$$

The resulting optimization problem is solved by minimizing the penalized SSE subject to the constraints of satisfying the quartic B-spline risk-neutral CDF conditions (10)–(16) and mean-forward price equality condition (20):

$$\begin{aligned} \min_{\mathbf{c},\boldsymbol{\theta}} L_\omega = {} & \sum_{i=1}^{N}(V(K_i) - V(K_i;\mathbf{c},\boldsymbol{\theta}))^2 \\ & + \omega\int_{K_1}^{K_N} [R'''(x;\mathbf{c},\boldsymbol{\theta})]^2 dx, \end{aligned} \tag{23}$$

$$\text{s.t. (10)–(16) and (20)},$$

where ω denotes a smoothing parameter.† The smoothing parameter represents the rate of exchange between the pricing error and roughness of the risk-neutral PDF.

It should be noted that the knots do not necessarily coincide with the traded strike prices since the option prices at

†We set the smoothness penalty parameter ω equal to 10^{-3}, which minimizes the RMISE of SML under the log-normal risk-neutral PDF.

the knot points are not required to estimate RNMs in the BSP method as shown in (23). Further, the number of knots (n) is not necessarily the same as the number of available prices (N). Thus, even if the strike prices are not equally spaced, we may apply the BSP method to estimate RNMs.

4.2. Three-step estimation procedure

The optimization problem (23) has two computational difficulties in estimating the RNM. The loss function in (23) is highly nonlinear due to the tail parameters, $\boldsymbol{\theta}$. It is computationally inefficient and inaccurate to estimate $\boldsymbol{\theta}$ and $\mathbf{c}$ simultaneously with a number of nonlinear constraints. Another problem is the choice of the optimum number of knots. A small number of knots may result in a function space that is not flexible enough to capture the true risk-neutral CDF. A large number may lead to serious overfitting. In order to avoid these problems, we develop the three-step estimation procedure:

- **Step 1:** Estimating the tail parameters, $\boldsymbol{\theta}$.
- **Step 2:** Selecting the optimum number of knots, n .
- **Step 3:** Estimating the control points, $\mathbf{c}$.

4.2.1. Estimation of power tail parameters

Since deep out-of-the-money option prices are almost determined by the shape of the risk-neutral CDF tails, the power tail parameters can be estimated using observed deep OTM option prices. The lower power tail parameters are estimated from the deep OTM put option prices. Under the lower power tail of the risk-neutral CDF, $\rho_1 x^{\lambda_1}$, the deep OTM put prices can be expressed as

$$\begin{aligned} P(K;\rho_1,\lambda_1) &= e^{-rT}\int_0^K (K-x)\rho_1\lambda_1 x^{\lambda_1-1}dx \\ &= e^{-rT}\frac{\rho_1}{\lambda_1+1}K^{\lambda_1+1}. \end{aligned}$$

Similarly, the upper tail of the risk-neutral CDF, $1-\rho_2 x^{-\lambda_2}$, can be estimated by deep OTM call option prices. The deep OTM call option prices are expressed as a function of the upper tail parameters:

$$\begin{aligned} C(K;\rho_2,\lambda_2) &= e^{-rT}\int_K^\infty (x-K)\rho_2\lambda_2 x^{-\lambda_2-1}dx \\ &= e^{-rT}\frac{\rho_2}{\lambda_2-1}K^{-\lambda_2+1}. \end{aligned}$$

As shown in (21) and (22), the tail parameters only affect the constant terms of the OTM option pricing function within the range $K_1 \le K \le K_N$. Therefore, in order to minimize the penalized SSE, the pricing errors at the end points, which are determined solely by the tail parameters, must be zero. Thus, the tail parameters can be estimated from the following optimization problems:

$$\min_{\rho_1,\lambda_1} \sum_{i=2}^{J} (P_i - P(K_i;\rho_1,\lambda_1))^2, \tag{24}$$

$$s.t.\ \ P_1 = e^{-rT}\frac{\rho_1}{\lambda_1+1}K_1^{\lambda_1+1},$$

and

$$\min_{\rho_2,\lambda_2} \sum_{i=1}^{J-1} (C_{N-J+i} - C(K_{N-J+i};\rho_2,\lambda_2))^2, \tag{25}$$

$$s.t.\ \ C_N = e^{-rT}\frac{\rho_2}{\lambda_2-1}K_N^{-\lambda_2+1}.$$

The pricing errors with power tails may increases as J increases, particularly when strike price intervals are large. If $J=2$, the solutions to the optimization problems (24) and (25) are expressed as

$$\lambda_1^* = \frac{\log(P_2/P_1)}{\log(K_2/K_1)} - 1,$$

$$\rho_1^* = e^{rT}\frac{(\lambda_1^*+1)P_1}{K_1^{\lambda_1^*+1}},$$

and

$$\lambda_2^* = 1 - \frac{\log(C_N/C_{N-1})}{\log(K_N/K_{N-1})},$$

$$\rho_2^* = e^{rT}\frac{(\lambda_2^*-1)C_N}{K_N^{-\lambda_2^*+1}}.$$

If the strike price intervals are small, we may use more than two OTM option prices to estimate the tail parameters.

4.2.2. Selection of the number of knots

With the estimated tail parameter vector, $\boldsymbol{\theta}^*$, the OTM option pricing function can be described only by the control points vector, $\mathbf{c}$:

$$V(K_i;\mathbf{c}|\boldsymbol{\theta}^*) = \min[C(K_i;\mathbf{c}|\boldsymbol{\theta}^*), P(K_i;\mathbf{c}|\boldsymbol{\theta}^*)], \quad i=1,\ldots,N,$$

where $\boldsymbol{\theta}^* = [\rho_1^*\rho_2^*\lambda_1^*\lambda_2^*]^{\mathrm{T}}$ is the RNM tail parameter vector that is pinned down in the first step. In order to estimate the control point vector, the number of knots, n, must be selected. A small number of knots may result in underfitting but, on the other hand, a large number may lead to serious overfitting. To select the optimal tradeoff between smoothness and fit, we choose the minimum number of knots, which attains zero bid–ask pricing errors, in constructing the B-spline risk-neutral CDF.

Define the bid–ask pricing errors as

$$e_i = (V_i^B - V(K_i;\mathbf{c}|\boldsymbol{\theta}^*))_+ + (V(K_i;\mathbf{c}|\boldsymbol{\theta}^*) - V_i^A)_+,$$

where V_i^B is the bid-quote OTM option price, V_i^A is the ask-quote OTM option price associated with the strike price K_i, and $x_+ = \max(0, x)$. If all the estimated OTM prices fall within the bid–ask price range, the sum of squared bid–ask pricing errors may be zero:

$$\min_{\mathbf{c}\in\mathbb{R}^{n-5}} \mathbf{e}^\top \mathbf{e} = 0, \tag{26}$$

where $\mathbf{e} = [e_1, \cdots, e_N]^{\mathrm{T}}$ is the bid–ask pricing error vector. To construct the B-spline risk-neutral CDF, we choose the minimum number of knots, n^*, satisfying the zero bid–ask pricing error condition (26):

$$n^* = \arg \min_{n\in z} n,$$

$$\text{s.t.}(26) \text{ with } (10)-(16) \text{ and}(20).$$

4.2.3. Estimation of the control points of B-splines

Once the tail parameter vector, $\boldsymbol{\theta}^*$, and the optimum number of knots, n^*, have been determined by steps 1 and 2, the nonlinear optimization problem (23) is expressed as a convex quadratic program that is efficiently solved by numerical optimization software. The optimization problem

$$\min_{\mathbf{c}\in\mathbf{R}^{n^*-5}} L_w = \sum_{i=1}^{N} (V(K_i) - V(K_i; \mathbf{c} \mid \boldsymbol{\theta}^*))^2 + \omega \int_{K_1}^{K_N} [R'''(x; \mathbf{c} \mid \boldsymbol{\theta}^*)]^2 dx,$$

$$\text{s.t. } (10)-(16) \text{ and } (20)$$

is equivalent to the following quadratic program:

$$\min_{\mathbf{c}\in\mathbb{R}^{n^*-5}} \tfrac{1}{2}\mathbf{c}^\top \mathbf{Q}\mathbf{c} + \mathbf{F}\mathbf{c}, \tag{27}$$

s.t.

(i) End point conditions

$$\begin{bmatrix} 1 & 11 & 11 & 1 & 0 & \dots & 0 & 0 & 0 & 0 & 0 \\ -1 & -3 & 3 & 1 & 0 & \dots & 0 & 0 & 0 & 0 & 0 \\ 1 & -1 & -1 & 1 & 0 & \dots & 0 & 0 & 0 & 0 & 0 \\ 0 & 0 & 0 & 0 & 0 & \dots & 0 & 1 & 11 & 11 & 1 \\ 0 & 0 & 0 & 0 & 0 & \dots & 0 & -1 & -3 & 3 & 1 \\ 0 & 0 & 0 & 0 & 0 & \dots & 0 & 1 & -1 & -1 & 1 \end{bmatrix}$$

$$\mathbf{c} = \begin{bmatrix} 24\rho_1^* K_1^{\lambda_1^*} \\ 6h\rho_1^*\lambda_1^* K_1^{\lambda_1^*-1} \\ 2h^2\rho_1^*\lambda_1^*(\lambda_1^*-1)K_1^{\lambda_1^*-2} \\ 24(1-\rho_2^* K_N^{-\lambda_2^*}) \\ 6h\rho_2^*\lambda_2^* K_N^{-\lambda_2^*-1} \\ -2h^2\rho_2^*\lambda_2^*(\lambda_2^*+1)K_N^{-\lambda_2^*-2} \end{bmatrix}.$$

(ii) Mean-forward price equality condition

$$\left[\int_{K_1}^{K_N} xB_{1,4}^{(1)}(x)dx \dots \int_{K_1}^{K_N} xB_{n-5,4}^{(1)}(x)dx\right]\mathbf{c} = S_0 e^{rT} - \frac{\rho_1^*\lambda_1^*}{\lambda_1^*+1}K_1^{\lambda_1^*+1} - \frac{\rho_2^*\lambda_2^*}{\lambda_2^*-1}K_N^{-\lambda_2^*+1}.$$

(iii) Non-negativity conditions

$$\begin{bmatrix} 0 & -1 & -3 & 3 & 1 & 0 & 0 & 0 & \dots & 0 \\ 0 & 0 & -1 & -3 & 3 & 1 & 0 & 0 & \dots & 0 \\ \vdots & \vdots & & \ddots & \ddots & \ddots & \ddots & \vdots & \vdots & \vdots \\ 0 & \dots & 0 & 0 & -1 & -3 & 3 & 1 & 0 & 0 \\ 0 & \dots & 0 & 0 & 0 & -1 & -3 & 3 & 1 & 0 \end{bmatrix}$$

$$\mathbf{c} \geqslant \mathbf{0},$$

where

$$\mathbf{Q} = \mathbf{G}^{\mathrm{T}}\mathbf{G} + \omega \mathbf{D}^{\mathrm{T}}\mathbf{R}\mathbf{D},$$

$$\mathbf{F} = -\mathbf{W}^{\mathrm{T}}\mathbf{G},$$

with

$$\mathbf{W} = \begin{bmatrix} P(K_1) + e^{-rT}\frac{\rho_1^*\lambda_1^*}{\lambda_1^*+1}K_1^{\lambda_1^*+1} \\ \vdots \\ P(K_p) + e^{-rT}\frac{\rho_1^*\lambda_1^*}{\lambda_1^*+1}K_1^{\lambda_1^*+1} \\ C(K_{p+1}) - e^{-rT}(\frac{\rho_2^*\lambda_2^*}{\lambda_2^*-1}K_N^{-\lambda_2^*+1} - K_{p+1}) \\ \vdots \\ C(K_N) - e^{-rT}(\frac{\rho_2^*\lambda_2^*}{\lambda_2^*-1}K_N^{-\lambda_2^*+1} - K_N) \end{bmatrix},$$

$$\mathbf{G} = \begin{bmatrix} \mathbf{M_1^{\mathrm{T}}} \\ \vdots \\ \mathbf{M_p^{\mathrm{T}}} \\ \mathbf{H_{p+1}^{\mathrm{T}}} \\ \vdots \\ \mathbf{H_N^{\mathrm{T}}} \end{bmatrix},$$

$$\mathbf{M_i} = e^{-rT}\begin{bmatrix} K_i B_{1,4}(K_i) - \int_{K_1}^{K_i} xB_{1,4}^{(1)}(x)dx \\ \vdots \\ K_i B_{n-5,4}(K_i) - \int_{K_1}^{K_i} xB_{n-5,4}^{(1)}(x)dx \end{bmatrix},$$

$$\mathbf{H_i} = e^{-rT}\begin{bmatrix} K_i B_{1,4}(K_i) + \int_{K_i}^{K_N} xB_{1,4}^{(1)}(x)dx \\ \vdots \\ K_i B_{n-5,4}(K_i) + \int_{K_i}^{K_N} x\, B_{n-5,4}^{(1)}(x)dx \end{bmatrix},$$

$$\mathbf{R} = \begin{bmatrix} \frac{h}{3} & \frac{h}{6} & 0 & 0 & \dots & 0 \\ \frac{h}{6} & \frac{2h}{3} & \frac{h}{6} & 0 & \dots & 0 \\ 0 & \frac{h}{6} & \ddots & \ddots & \ddots & \vdots \\ 0 & 0 & \ddots & \ddots & \frac{h}{6} & 0 \\ \vdots & \vdots & \ddots & \frac{h}{6} & \frac{2h}{3} & \frac{h}{6} \\ 0 & 0 & \dots & 0 & \frac{h}{6} & \frac{h}{3} \end{bmatrix},$$

$$\mathbf{D} = \begin{bmatrix} B_{1,4}^{(3)}(x_5) & \cdots & B_{n-5,4}^{(3)}(x_5) \\ \vdots & \vdots & \vdots \\ B_{1,4}^{(3)}(x_{(n-4)}) & \cdots & B_{n-5,4}^{(3)}(x_{n-4}) \end{bmatrix},$$

$$B_{i,4}^{(3)}(x) = \left(\frac{z_i}{h^3}\right) I_{[x_i, x_{i+1})}(x) + \left(\frac{-4z_i + 5}{h^3}\right) I_{[x_{i+1}, x_{i+2})}(x) + \left(\frac{6z_i - 15}{h^3}\right) I_{[x_{i+2}, x_{i+3})}(x) + \left(\frac{-4z_i + 15}{h^3}\right) I_{[x_{i+3}, x_{i+4})}(x) + \left(\frac{z_i - 5}{h^3}\right) I_{[x_{i+4}, x_{i+5})}(x),$$

$$z_i = (x - x_i)/h, h = x_{i+1} - x_i.$$

The derivation of the quadratic program (27) is given in appendix B.

The simple three-step estimation procedure results in a solution that is very close to, but not quite the same as, the solution to the optimization problem (23). In order to obtain more accurate solutions to (23), we need to iterate steps 1 and 3 by applying the Newton–Raphson method as follows:†

$$\boldsymbol{\theta}^{(n+1)} = \boldsymbol{\theta}^{(n)} - \left[\frac{\partial^2 L(\boldsymbol{\theta}^{(n)})}{\partial \boldsymbol{\theta}^{(n)} \partial \boldsymbol{\theta}^{(n)^{\mathrm{T}}}}\right]^{-1} \frac{\partial L(\boldsymbol{\theta}^{(n)})}{\partial \boldsymbol{\theta}^{(n)}}, \quad \boldsymbol{\theta}^{(0)} = \boldsymbol{\theta}^*,$$

where

$$L(\boldsymbol{\theta}) := \min_{\mathbf{c}} L_\omega(\mathbf{c}|\boldsymbol{\theta}), \quad \text{s.t.} (10) - (16) \text{ and } (20).$$

5. Comparison results

5.1. Recovering the risk-neutral PDF

In this section, we compare our quartic B-spline risk-neutral CDF (BSP) method and the SML method with respect to their flexibility in recovering hypothetical actual risk-neutral PDFs. A good RNM estimation technique should be able to recover the true RNMs whatever the complexity of their shape. Therefore, to compare the ability to recover a wide range of different PDF shapes, the following 12 parametric PDFs are assumed to be an actual risk-neutral PDF.‡

(1) Log-normal distribution (LN).
(2) Log-stable distribution (LS).
(3) Double log-normal distribution (DN).
(4) Double log-stable distribution (DS).
(5) Generalized log-stable distribution (GS).
(6) Weibull distribution (WB).
(7) Generalized gamma distribution (GG).
(8) Generalized beta distribution (GB).
(9) Finite moment log-stable distribution (FS).
(10) Variance gamma distribution (VG).
(11) Poisson jump diffusion process (JD).
(12) Jump diffusion process with stochastic volatility (VG).

The closed-form PDFs or characteristic functions for the 12 models are given in appendix C.

First, 12 cross-sections of OTM option prices are generated from each hypothetical actual risk-neutral PDF. The OTM option prices $V(K_i)$, $i = 1, 2, \dots, N$, are calculated at equally spaced strike prices $K_1 < \cdots < K_N$ with $K_{i+1} - K_i = \Delta K$§ for each hypothetical actual risk-neutral PDF using the call and put option price functions

$$C(K_i) = e^{-rT} \int_{K_i}^{\infty} (x - K_i) p(x) dx,$$

$$P(K_i) = e^{-rT} \int_{0}^{K_i} (K_i - x) p(x) dx,$$

$$V(K_i) = \min[C(K_i), P(K_i)],$$

where r is the risk-free rate, T is the time to maturity, and $p(x)$ is the actual risk-neutral PDF. The parameters of the hypothetical actual distributions are chosen to approximate a typical cross-section of OTM option prices on the S&P 500 index with 2 months to maturity.

†Monte-Carlo simulation shows that this iteration reduces only about 0.001% of RMISE, but significantly increases the computational burden. This implies that the simple three-step estimation procedure is considerably accurate and the improvement by iteration is negligible.

‡The risk-neutral PDF at maturity can be inferred from the stochastic process. The risk-neutral PDF of the stochastic process is obtained by inverting its characteristic function. In order to find examples of the jump-diffusion process and stochastic volatility models, see Bakshi *et al.* (1997) and Carr and Wu (2003).

§In our experiment we generate the OTM option prices $V(K_i)$ for 25 strikes K_i in the interval [1100, 1800].

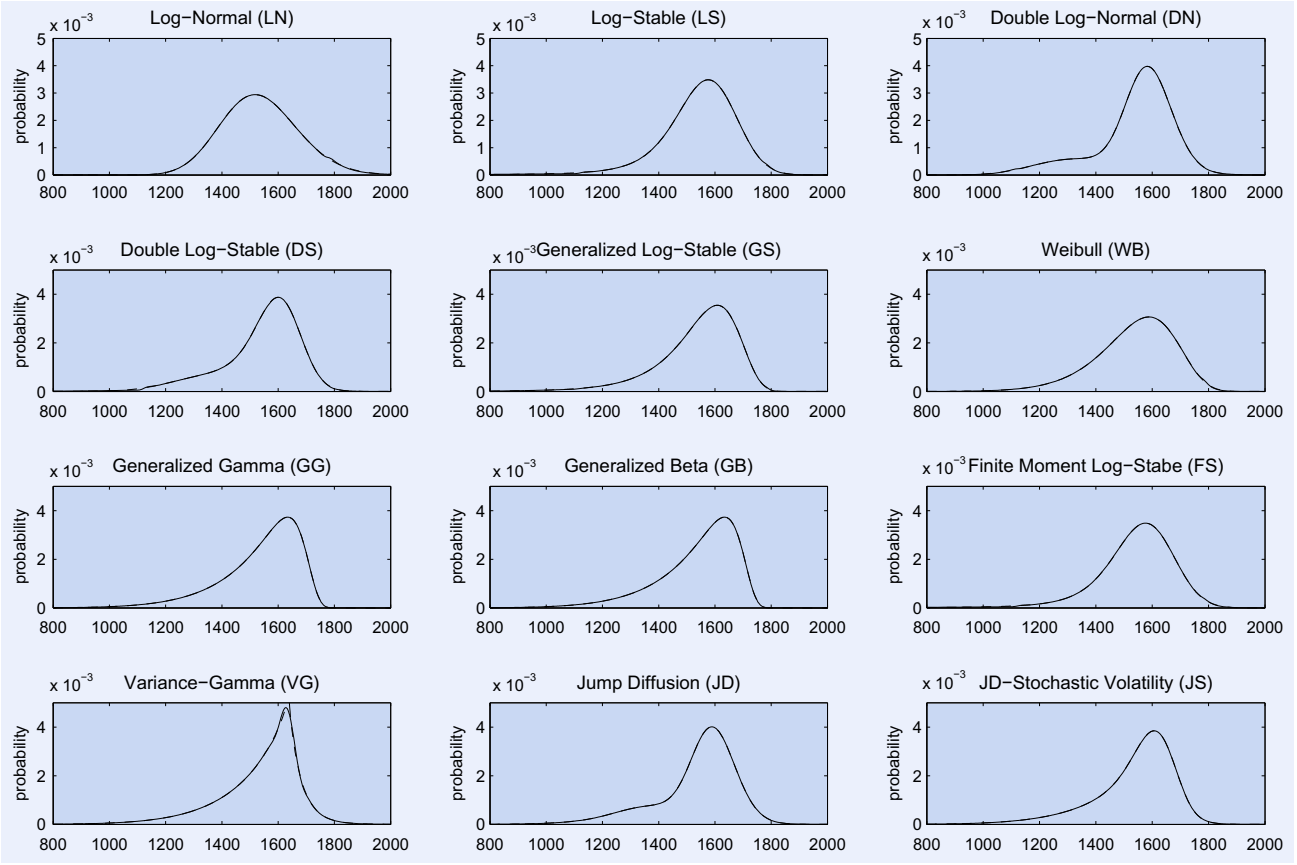

Figure 3. BSP method: Recovering the hypothetical actual risk-neutral PDF. The dashed lines are actual risk-neutral PDFs and the solid lines are risk-neutral PDFs recovered by the BSP method.

With the generated OTM option prices, we then recover the actual risk-neutral PDF using the BSP method and SML method, respectively. Finally, we measure the closeness between the actual distribution P and the recovered distribution Q by means of Kullback–Leibler Information Criterion (KLIC) divergence:†

$$D_{KL}(P \parallel Q) = \int_0^\infty p(x) \log \frac{p(x)}{q(x)}\, dx,$$

where $p(x)$ and $q(x)$ denote the PDFs of the actual distribution P and the recovered distribution Q, respectively.

The recovered risk-neutral PDFs are plotted against each actual risk-neutral PDF for the BSP method in Figure 3 and for the SML method in Figure 4. These figures suggest that the BSP method is more flexible than the SML method in recovering the actual distributions. The BSP method almost perfectly recovers the actual risk-neutral PDFs for all hypothetical distributional assumptions. In contrast, the SML method is significantly biased and gives negative probability, particularly for some fat-tailed distributions such as stable distributions: LS, DS, and GS. The KLIC divergences between the actual and recovered risk-neutral PDFs for each method are reported in Table 1. The KLIC divergences of the BSP method are much smaller than those of the SML method except for cases where the actual risk-neutral PDF is log-normal or double log-normal. The SML method performs slightly better than the BSP method if the true RNM is a thin-tailed distribution such as log-normal or double log-normal. This is because the volatility smile of the thin-tailed RNM is very flat and thus the smile approximation errors of the tail parts are smaller than those of the fat-tailed RNM.

5.2. Monte-Carlo experiments

In the previous section, we only compare the accuracy of the two methods using the theoretical OTM option prices which are generated with no pricing errors from the 12 different hypothetical actual risk-neutral PDFs. However, stability to pricing errors is also a desirable property of a good RNM estimation method. Therefore, in this section we perform Monte-Carlo experiments to compare both the accuracy and stability of the two methods in the RNM estimation. To test the robustness of alternative methods to pricing errors embedded in OTM option prices, we add

†Kullback–Leibler divergence is a measure of the difference between two probability distributions: from a 'true' probability distribution to an arbitrary probability distribution (Kullback and Leibler 1951). Although it is often interpreted as a distance metric, the KL divergence is not a true metric since it is not symmetric (hence 'divergence' rather than 'distance').

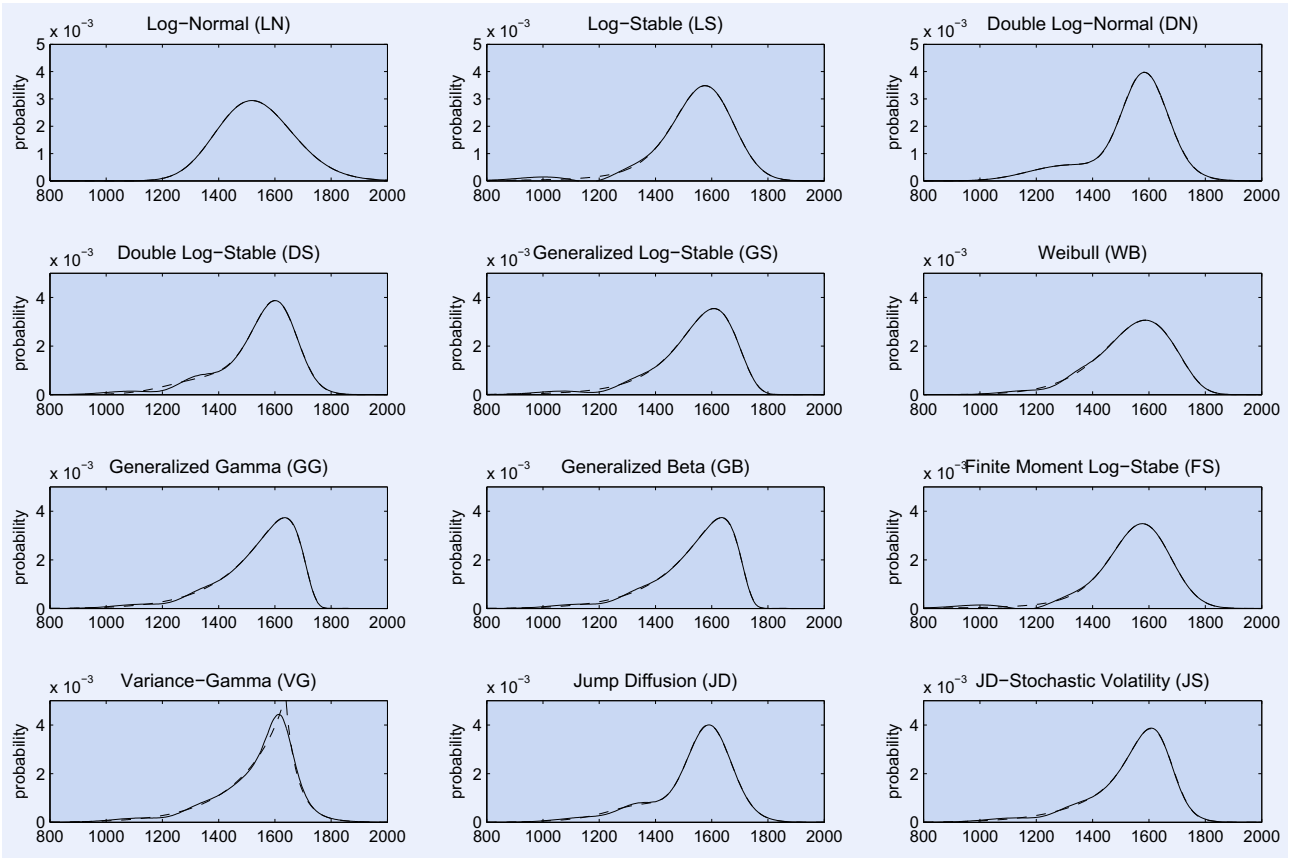

Figure 4. SML method: Recovering the hypothetical actual risk-neutral PDF. The dashed lines are actual risk-neutral PDFs and the solid lines are risk-neutral PDFs recovered by the SML method.

Table 1. Kullback–Leibler information criterion (KLIC) divergence. The KLIC divergences are computed based on the 12 hypothetical actual risk-neutral PDFs for each method.

Actual RNM	BSP method	SML method
LN	0.0006	0.0000
LS	0.0013	0.0305
DN	0.0001	0.0000
DS	0.0013	0.0073
GS	0.0000	0.0042
WB	0.0002	0.0019
GG	0.0000	0.0020
GB	0.0000	0.0020
FS	0.0013	0.0305
VG	0.0004	0.0050
JD	0.0000	0.0016
JS	0.0000	0.0019
AVG	0.0004	0.0072

noise ϵ_i to the theoretical prices computed in the previous section. Pricing errors ϵ_i are introduced to model observational errors that arise from market imperfections such as non-synchronicity, bid–ask spread, discreteness, etc.

As pointed out by Anderson and Lomakka (2005), the option pricing errors exhibit dependence and heteroscedasticity over the range of strike prices. To take into account the dependency and heteroscedastic characteristics in the pricing error structures, we specify the pricing errors as a random walk process bounded by the maximum bid–ask spread permitted by the exchange, which is a function of the option prices:

$$\epsilon_i = \max[\min(\epsilon_{i-1} + \xi_i, 0.5s_i), -0.5s_i],$$
$$i = 1, \ldots, N,\ \epsilon_0 = 0,$$

where ξ_i is independently and uniformly distributed on $[-0.5s_i, 0.5s_i]$, and s_i is the maximum bid–ask spread which

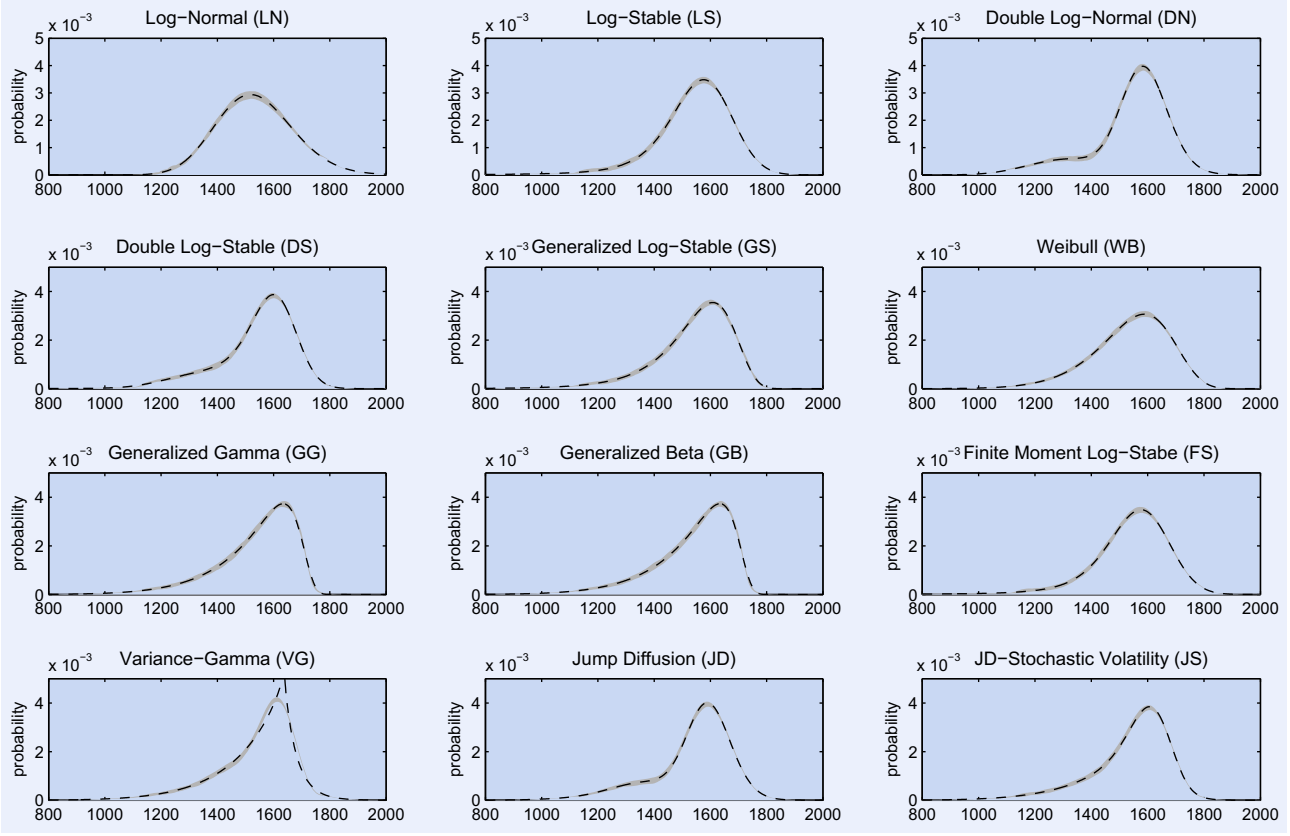

Figure 5. BSP method: Monte-Carlo experiments. The dashed lines are true risk-neutral PDFs and the grey areas are the ranges of estimated risk-neutral PDFs recovered by the BSP method.

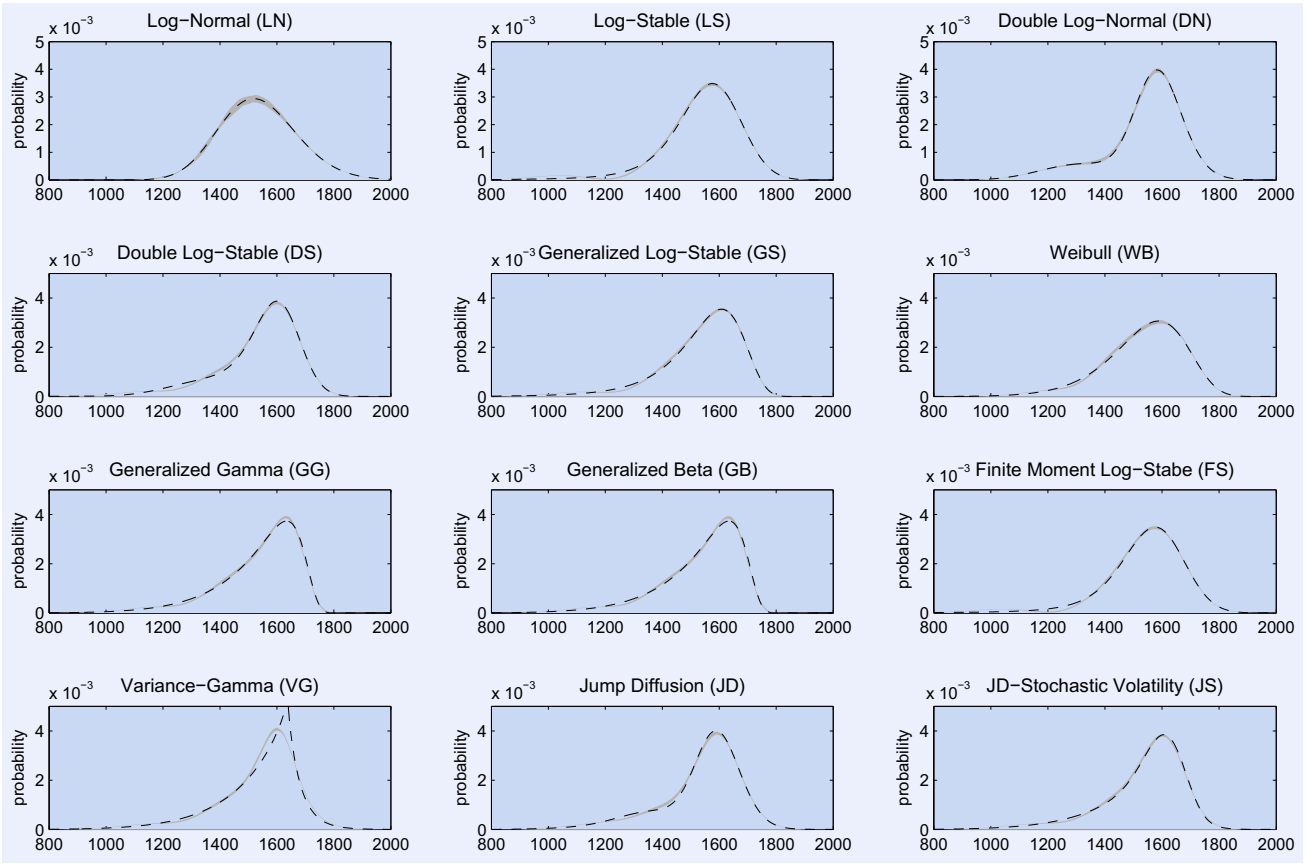

Figure 6. SML method: Monte-Carlo experiments. The dashed lines are true risk-neutral PDFs and the grey areas are the ranges of estimated risk-neutral PDFs recovered by the SML method.

Table 2. Root mean integrated squared errors (RMISE). The RMISE is decomposed as $\mathrm{RMISE}^2(\hat{p}) = \mathrm{RISB}^2(\hat{p}) + \mathrm{RIV}^2(\hat{p})$. The RMISEs are computed based on 500 simulated sets of cross-section data on S&P 500 index options with 2 months to maturity under the 12 scenarios for each method.

Scenario	BSP method RMISE	RISB	RIV	SML method RMISE	RISB	RIV
LN	0.0229	0.0091	0.0210	0.0194	0.0024	0.0192
LS	0.0200	0.0068	0.0188	0.0466	0.0459	0.0082
DN	0.0213	0.0114	0.0180	0.0192	0.0162	0.0102
DS	0.0233	0.0149	0.0180	0.0502	0.0495	0.0087
GS	0.0253	0.0116	0.0225	0.0373	0.0363	0.0087
WB	0.0189	0.0048	0.0183	0.0350	0.0333	0.0105
GG	0.0304	0.0204	0.0226	0.0422	0.0410	0.0101
GB	0.0309	0.0207	0.0229	0.0419	0.0407	0.0099
FS	0.0199	0.0068	0.0187	0.0465	0.0458	0.0081
VG	0.1214	0.1202	0.0175	0.1593	0.1591	0.0087
JD	0.0223	0.0138	0.0176	0.0440	0.0430	0.0096
JS	0.0229	0.0134	0.0185	0.0379	0.0368	0.0090
AVG	0.0316	0.0211	0.0195	0.0483	0.0458	0.0101

Table 3. Comparison between the BSP and SML methods with respect to non-negativity, sum-to-unity and mean-forward price equality. The comparisons are conducted based on cross-section data on 30–60 days to maturity S&P 500 index options from January 4 to March 31, 2010.

Criterion	BSP method Mean	Min	Max	SML method Mean	Min	Max
$\int_0^\infty \lvert \min(\hat{p}(x), 0)\rvert dx$	0.0000	0.0000	0.0000	0.0004	0.0000	0.0028
$\lvert\int_0^\infty \hat{p}(x)dx - 1\rvert$	0.0000	0.0000	0.0000	0.0004	0.0000	0.0028
$\lvert\int_0^\infty x\hat{p}(x)dx - S_0 e^{(r-d)T}\rvert$	0.0006	0.0000	0.0067	0.3664	0.0000	2.4494

depends on the strike K_i.† In the experiment, the actual risk-neutral PDFs are modeled by 12 parametric distributions as in the previous section. The parameters of these distributions are chosen to fit a randomly selected cross-section from the S&P 500 index options dataset. For a given actual risk-neutral PDF, we simulate 500 cross-sections of OTM option prices with pricing errors for each scenario and apply the two methods to estimate the corresponding risk-neutral PDFs.

We measure the accuracy and stability of the RNM estimators by means of the root mean integrated squared errors (RMISE) criterion as in Bondarenko (2003). Let $\hat{p}(x)$ be the estimator of risk-neutral density $p(x)$, then the (normalized) RMISE for the density estimator is defined as

$$\mathrm{RMISE}(\hat{\mathrm{p}}) = \frac{1}{\| \mathrm{p}(x) \|}(E[\| \hat{\mathrm{p}}(x) - \mathrm{p}(x) \|^2])^{1/2}$$

$$= \frac{1}{\| p(x) \|}\left(E\left[\int_0^\infty (\hat{\mathrm{p}}(x) - \mathrm{p}(x))^2 \mathrm{d}x\right]\right)^{1/2}.$$

Similarly to the MSE for the point estimator, the RMISE may be decomposed as

$$\mathrm{RMISE}^2(\hat{\mathrm{p}}) = \mathrm{RISB}^2(\hat{\mathrm{p}}) + \mathrm{RIV}^2(\hat{\mathrm{p}}),$$

where

$$\mathrm{RISB}(\hat{p}) = \frac{1}{\| \mathrm{p}(x) \|}\left(\int_0^\infty (E[\hat{\mathrm{p}}(x)] - \mathrm{p}(x))^2 \mathrm{d}x\right)^{1/2},$$

$$\mathrm{RIV}(\hat{p}) = \frac{1}{\| p(x) \|}\left(\int_0^\infty E[(\hat{\mathrm{p}}(x) - E[\hat{\mathrm{p}}(x)])^2] \mathrm{d}x\right)^{1/2},$$

$\| \cdot \|$ is the L_2 norm, RISB is the (normalized) root integrated squared bias, and RIV is the (normalized) root integrated variance. Intuitively, RMISE is a measure of the overall quality of the estimator, RISB is a measure of the accuracy, and RIV is a measure of the stability. This decomposition allows us to study the relative contributions of the bias (RISB) and the variability (RIV) to RMISE of different models.

Monte-Carlo experiments are conducted based on the following 12 scenarios:

Scenario $i : i$ distribution is the true risk − neutral PDF,

where $i =$ *LN*, LS, DN, DS, GS, WB, GG, GB, FS, VG, JD, and JS. The resulting true risk-neutral PDFs, $p(x)$, for each scenario are depicted by the dashed lines in Figures 5 and 6, respectively. For each scenario, the estimated 500 risk-neutral PDFs by the two methods are plotted against their true risk-neutral PDFs in Figures 5 and 6, respectively. It can be seen that the SML is significantly biased, particularly on the lower tail of the distribution. The associated RMISE statistics for the 12 scenarios are also presented in Table 2. The results for the BSP method are displayed in the left panel. Examining the RMISE statistics from the two methods, we find that the BSP provides lower RMISE than the SML in most scenarios except for LN and DN. In particular, under the scenarios where the true RNM is a fat-tailed distribution such as LS, DS, FS, and GS, the SML method exhibits large biases from the true risk-neutral PDFs. These results indicate the better overall quality of the BSP as a RNM estimator. Examining the RISB and the RIV reveals that the large bias from the true risk-neutral PDF is the main cause of the relatively poor performance of the SML method.

5.3. Application to S&P 500 index options

5.3.1. Data

In order to address the robustness of the RNM estimation methods, we apply the two methods to real market data. We estimate the risk-neutral density using the cross-section data on the S&P 500 index options traded at the Chicago Board of Options Exchange (CBOE). The RNM estimations are based on a database containing European option quotes on the S&P 500 index from January 4 to March 31, 2010. The transaction prices are recorded with substantial measurement errors due to non-synchronous trading so that we use daily closing bid and ask price quotes. We obtain 52 sets of cross-section data on the S&P 500 index options that have 30–60 days to maturity. The reason for choosing options that have 30–60 days to maturity is that they are the most liquid data among various maturities.‡ The data are filtered by checking the arbitrage violation conditions such as the monotonicity and convexity of the option prices. Since risk-free interest

†The maximum bid–ask spread permitted by the exchange is linked to the option quotes. For instance, the CBOE rules state that the maximum bid–ask spread is 1/4 for options with bid quote below \$2, 3/8 for bid quotes between \$2 and \$5, 1/2 for bid quotes between \$5 and \$10, and so on

$$s_i = M(K_i)$$

The function $M(\cdot)$ is constructed to represent such rules. See Bondarenko (2003) for details on the construction of $M(\cdot)$.

‡As Buraschi and Jackwerth (2001) pointed out, most of the trading activity in S&P 500 options is concentrated in the nearest (0–30 days to maturity) and second nearest (30–60 days to maturity) contracts. Options that expire within 30 days are excluded from the sample because of abnormal trading volumes for options close to expiry reported by Stoll and Whaley (1987).

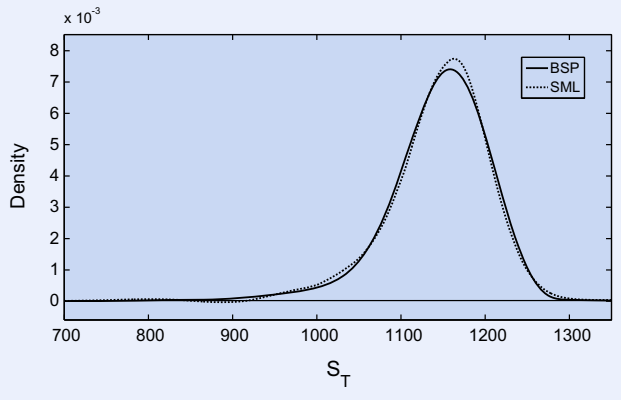

Figure 7. Estimated RNM densities for 40 days to maturity S&P 500 index options on March 9, 2010.

rates for a time of maturity exactly matching the options' time to maturity generally cannot be observed, we compute implied risk-free interest rates embedded in the European put–call parity as suggested by Jackwerth and Rubinstein (1996).

5.3.2. *Results*

Figure 7 illustrates the risk-neutral PDFs estimated by the BSP method and SLM method for 40 days to maturity options on March 9, 2010. The risk-neutral PDF estimated by the SML method has negative probabilities in the lower tail, roughly between 850 and 910, while the risk-neutral PDF estimated by the BSP method satisfies the non-negativity condition.

We estimate the risk-neutral PDFs using the BSP and SML methods, respectively, for each cross-section data set from January 4 to March 31, 2010 in order to compare the two methods with respect to the following criteria:†

(i) Non-negativity condition: $\int_0^\infty |\min(\hat{p}(x), 0)| \, \mathrm{d}x = 0$.
(ii) Sum-to-unity condition: $\int_0^\infty \hat{p}(x) \mathrm{d}x = 1$.
(iii) Mean-forward price equality condition: $\int_0^\infty x\hat{p}(x) \, \mathrm{d}x = S_0 e^{(r-d)T}$.

Table 3 reports the comparison results of the two methods with respect to the three criteria. The BSP method outperforms the SML method with respect to all the criteria. The BSP method almost meets the three conditions with very small errors in the mean-forward price equality condition, while the SML method violates them with considerable errors. Thus, our application to real market data also confirms the Monte-Carlo simulation results.

6. Conclusion

In this paper, we propose a new RNM estimation method that overcomes the problems encountered with the smoothed implied volatility smile (SML) method. In our new approach, we model the risk-neutral CDF using quartic B-splines with power tails. With the power tails, the estimated RNM has non-negative tail probabilities and also reflects information about true tail probabilities. Since the risk-neutral CDFs are constructed using quartic B-spline functions, the resulting risk-neutral PDFs have continuity C^2. The use of the B-spline also improves the computational efficiency and reduces the number of spline parameters. The advantage of constructing the risk-neutral CDF with power tails is that the sum of RNM probabilities is guaranteed to be unity. We also choose the optimum number of knots so that our method avoids both overfitting and oversmoothing.

Our approach involves solving a highly nonlinear optimization problem with a number of constraints due to the power tails. It is computationally difficult and inaccurate to estimate the B-spline part of the CDF and the power tails simultaneously. To improve the computational efficiency and accuracy we develop the three-step RNM estimation technique: (i) estimate the power tail parameters; (ii) select the optimum number of knots; and (iii) estimate the B-spline control points. The three-step estimation procedure transforms a nonlinear optimization problem into a convex quadratic programming that is efficiently solved by numerical optimization software.

Monte-Carlo experiments suggest that the BSP method performs considerably better than the SML method as a technique for estimating option implied RNM. The SML method violates the no-arbitrage conditions, and is also significantly biased, particularly under scenarios where the true RNM is a fat-tailed distribution. In contrast, the BSP method always produces arbitrage-free RNM estimators, and almost perfectly recovers the actual risk-neutral PDFs for all hypothetical distributions. Application to the S&P 500 index options also confirms the Monte-Carlo simulation results.

Finally, we developed the BSP method to address the drawbacks of the SML method by using spline functions in a different way and thus have compared the BSP method only with the SML method. Further research is needed to compare the BSP method with various parametric and non-parametric RNM estimation methods.

Acknowledgements

The author is grateful to J. Huston McCulloch for his invaluable comments and advice. The author also thanks P. Evans, P.S. Lam, and R. Kimmel for helpful comments.

†Since the BSP and SML methods are always capable of producing an exact fit to the data by decreasing the smoothing parameter (w) or increasing the number of knots (n), we do not compare the goodness-of-fit of the two methods.

References

Anderson, M. and Lomakka, M., Evaluating implied RNDs by some new confidence interval estimation techniques. *J. Bank. Finance*, 2005, **29**, 1535–1557.

Bakshi, G., Cao, C. and Chen, Z., Empirical performance of alternative option pricing models. *J. Finance*, 1997, **52**, 2003–2049.

Bliss, R. and Panigirtzoglou, N., Testing the stability of implied probability density functions. *J. Bank. Finance*, 2002, **26**, 381–422.

Bondarenko, O., Estimation of risk neutral densities using positive convolution approximation. *J. Econometr.*, 2003, **116**, 85–112.

Breeden, D. and Litzenberger, R., Prices of state contingent claims implicit in option prices. *J. Business*, 1978, **51**, 621–652.

Bu, R. and Hadry, K., Estimating option implied risk-neutral densities using spline and hypergeometric functions. *Econometr. J.*, 2007, **10**, 216–244.

Buraschi, A. and Jackwerth, J., The price of a smile: hedging and spanning in option markets. *Rev. Financ. Stud.*, 2001, **14**, 495–527.

Campa, J.M., Chang, P.H.K. and Reider, R.L., Implied exchange rate distributions: evidence from OTC option markets. *J. Int. Money Finance*, 1998, **17**, 117–160.

Carr, P. and Wu, L., Finite moment log stable process and option pricing. *J. Finance*, 2003, **58**, 753–777.

Carr, P. and Wu, L., Variance risk premia. *Rev. Financ. Stud.*, 2009, **22**(3), 1311–1341.

Cox, J. and Ross, S., The valuation of options for alternative stochastic processes. *J. Financ. Econ.*, 1976, **3**, 145–166.

de Boor, C., *A Practical Guide to Splines*, 1978 (Springer: Berlin).

Fengler, M.R., Arbitrage-free smoothing of the implied volatility surface. *Quant. Finance*, 2009, **9**(4), 417–428.

Fisher, M.E., Nychka, D. and Zervos, D., Fitting the term structure of interest rates with smoothing splines. Working Paper, Board of Governors of the Federal Reserve System, 1995.

Jackwerth, J. and Rubinstein, M., Recovering probability distributions from option prices. *J. Finance*, 1996, **51**, 1611–1631.

Jiang, G.J. and Tian, Y.S., Model-free implied volatility and its information content. *Rev. Financ. Stud.*, 2005, **18**(4), 1305–1342.

Jiang, G.J. and Tian, Y.S., Extracting model-free volatility from option prices: an examination of the VIX index. *J. Deriv.*, 2007, Spring, 1–26.

Kullback, S. and Leibler, R.A., On information and sufficiency. *Ann. Math. Statist.*, 1951, **22**, 79–86.

Malz, A.M., Estimating the probability distribution of the future exchange rate from options prices. *J. Deriv.*, 1997, **5**, 18–36.

McCulloch, J.H., Measuring the term structure of interest rates. *J. Business*, 1971, **44**, 19–31.

McCulloch, J.H., The tax-adjusted yield curve. *J. Finance*, 1975, **30**, 811–830.

Monterio, A.M., Tütüncü, R. and Vicente, L.N., Recovering risk-neutral probability density functions from options prices using cubic splines and ensuring nonnegativity. *Eur. J. Oper. Res.*, 2008, **187**, 525–542.

Panigirtzoglou, N. and Skiadopoulos, G., A new approach to modeling the dynamics of implied distribution: theory and evidence from the S&P500 options. *J. Bank. Finance*, 2004, **28**, 1499–1520.

Ross, S., Options and efficiency. *Q. J. Econ.*, 1976, **90**, 75–89.

Shimko, D.C., Bounds of probability. *Risk*, 1993, **6**, 33–37.

Stoll, H.R. and Whaley, R.E., Program trading and expiration-day effects. *Financ. Anal. J.*, 1987, **43**, 16–28.

Stutzer, M., A simple nonparametric approach to derivative security valuation. *J. Finance*, 1996, **51**, 1633–1652.

Appendix A: Derivation of the option price functions under the B-spline RNM CDF with power tails

A.1. The case $K < K_1$

$$
\begin{aligned}
C(K;\mathbf{c},\boldsymbol{\theta}) &= e^{-rT}\int_K^\infty xR'(x)\mathrm{d}x - Ke^{-rT}\int_K^\infty R'(x)\mathrm{d}x \\
&= e^{-rT}\int_K^{K_1}\rho_1\lambda_1 x^{\lambda_1}\mathrm{d}x + e^{-rT}\int_{K_1}^{K_N} x\sum_{i=1}^{n-5}c_iB_{i,4}^{(1)}(x)\mathrm{d}x \\
&\quad + e^{-rT}\int_{K_N}^\infty \rho_2\lambda_2 x^{-\lambda_2}\mathrm{d}x - Ke^{-rT}(1-\rho_1K^{\lambda_1}) \\
&= e^{-rT}\frac{\rho_1\lambda_1}{\lambda_1+1}(K_1^{\lambda_1+1}-K^{\lambda_1+1}) \\
&\quad + e^{-rT}\int_{K_1}^{K_N} x\sum_{i=1}^{n-5}c_iB_{i,4}^{(1)}(x)\mathrm{d}x + e^{-rT}\frac{\rho_2\lambda_2}{\lambda_2-1}K_N^{-\lambda_2+1} \\
&\quad - Ke^{-rT}(1-\rho_1K^{\lambda_1}) = e^{-rT}\left[\sum_{i=1}^{n-5}c_i\int_K^{K_N}xB_{i,4}^{(1)}(x)\mathrm{d}x\right. \\
&\quad \left. + \frac{\rho_1\lambda_1}{\lambda_1+1}K_1^{\lambda_1+1} + \frac{\rho_2\lambda_2}{\lambda_2-1}K_N^{-\lambda_2+1} + \frac{\rho_1}{\lambda_1+1}K^{\lambda_1+1} - K\right],
\end{aligned}
\tag{A1}
$$

$$
\begin{aligned}
P(K;\mathbf{c},\boldsymbol{\theta}) &= -e^{-rT}\int_0^K xR'(x)\mathrm{d}x + Ke^{-rT}\int_0^K R'(x)\mathrm{d}x \\
&= -e^{-rT}\int_0^K \rho_1\lambda_1 x^{\lambda_1}\mathrm{d}x + Ke^{-rT}(\rho_1K^{\lambda_1}) \\
&= e^{-rT}\left[-\frac{\rho_1\lambda_1}{\lambda_1+1}K^{\lambda_1+1} + \rho_1K^{\lambda_1+1}\right] \\
&= e^{-rT}\frac{\rho_1}{\lambda_1+1}K^{\lambda_1+1}.
\end{aligned}
\tag{A2}
$$

A.2. The case $K_1 \le K \le K_N$

$$
\begin{aligned}
C(K;\mathbf{c},\boldsymbol{\theta}) &= e^{-rT}\int_K^\infty xR'(x)\mathrm{d}x - Ke^{-rT}\int_K^\infty R'(x)\mathrm{d}x \\
&= e^{-rT}\int_K^{K_N} x\sum_{i=1}^{n-5}c_iB_{i,4}^{(1)}(x)\mathrm{d}x + e^{-rT} \\
&\quad \times \int_{K_N}^\infty \rho_2\lambda_2 x^{-\lambda_2}\mathrm{d}x \\
&\quad - Ke^{-rT}\left(1-\sum_{i=1}^{n-5}c_iB_{i,4}(K)\right) \\
&= e^{-rT}\sum_{i=1}^{n-5}c_i\int_K^{K_N}xB_{i,4}^{(1)}(x)\mathrm{d}x \\
&\quad + e^{-rT}\frac{\rho_2\lambda_2}{\lambda_2-1}K_N^{-\lambda_2+1} - Ke^{-rT} \\
&\quad + e^{-rT}\left(\sum_{i=1}^{n-5}c_iKB_{i,4}(K)\right) \\
&= e^{-rT}\left[\sum_{i=1}^{n-5}c_i(KB_{i,4}(K) + \int_K^{K_N}xB_{i,4}^{(1)}(x)\mathrm{d}x)\right. \\
&\quad \left. + \frac{\rho_2\lambda_2}{\lambda_2-1}K_N^{-\lambda_2+1} - K\right],
\end{aligned}
\tag{A3}
$$

$$P(K;\mathbf{c},\boldsymbol{\theta}) = -e^{-rT}\int_0^K xR'(x)\mathrm{d}x + Ke^{-rT}\int_0^K R'(x)\mathrm{d}x$$
$$= -e^{-rT}\int_0^{K_1}\rho_1\lambda_1 x^{\lambda_1}\mathrm{d}x - e^{-rT}\int_{K_1}^K x\sum_{i=1}^{n-5}c_iB_{i,4}^{(1)}(x)\mathrm{d}x$$
$$+ Ke^{-rT}\sum_{i=1}^{n-5}c_iB_{i,4}(K) = -e^{-rT}\frac{\rho_1\lambda_1}{\lambda_1+1}K_1^{\lambda_1+1}$$
$$- e^{-rT}\sum_{i=1}^{n-5}c_i\int_{K_1}^K xB_{i,4}^{(1)}(x)\mathrm{d}x + Ke^{-rT}\sum_{i=1}^{n-5}c_iB_{i,4}(K)$$
$$= e^{-rT}\left[\sum_{i=1}^{n-5}c_i(KB_{i,4}(K) - \int_{K_1}^K xB_{i,4}^{(1)}(x)dx) - \frac{\rho_1\lambda_1}{\lambda_1+1}K_1^{\lambda_1+1}\right]. \quad \text{(A4)}$$

A.3. The case $K_N < K$

$$C(K;\mathbf{c},\boldsymbol{\theta}) = e^{-rT}\int_K^\infty xR'(x)\mathrm{d}x - Ke^{-rT}\int_K^\infty R'(x)\mathrm{d}x$$
$$= e^{-rT}\int_K^\infty \rho_2\lambda_2 x^{-\lambda_2}\mathrm{d}x - Ke^{-rT}(1-(1$$
$$-\rho_2K^{-\lambda_2}))$$
$$= e^{-rT}\left[\frac{\rho_2\lambda_2}{\lambda_2-1}K^{-\lambda_2+1} - \rho_2K^{-\lambda_2+1})\right]$$
$$= e^{-rT}\frac{\rho_2}{\lambda_2-1}K^{-\lambda_2+1}, \quad \text{(A5)}$$

$$P(K;\mathbf{c},\boldsymbol{\theta}) = -e^{-rT}\int_0^K xR'(x)\mathrm{d}x + Ke^{-rT}\int_0^K R'(x)\mathrm{d}x$$
$$= -e^{-rT}\int_0^{K_1}\rho_1\lambda_1 x^{\lambda_1}\mathrm{d}x - e^{-rT}\int_{K_1}^{K_N} x\sum_{i=1}^{n-5}c_iB_{i,4}^{(1)}(x)\mathrm{d}x$$
$$- e^{-rT}\int_{K_N}^K \rho_2\lambda_2 x^{-\lambda_2}\mathrm{d}x + Ke^{-rT}(1-\rho_2K^{-\lambda_2})$$
$$= -e^{-rT}\frac{\rho_1\lambda_1}{\lambda_1+1}K_1^{\lambda_1+1} - e^{-rT}\sum_{i=1}^{n-5}c_i\int_{K_1}^K xB_{i,4}^{(1)}(x)\ \mathrm{d}x$$
$$+ e^{-rT}\frac{\rho_2\lambda_2}{\lambda_2-1}(K^{-\lambda_2+1} - K_N^{-\lambda_2+1}) + e^{-rT}(K - \rho_2K^{-\lambda_2+1})$$
$$= e^{-rT}\left[-\sum_{i=1}^{n-5}c_iKB_{i,4}(K) - \frac{\rho_1\lambda_1}{\lambda_1+1}K_1^{\lambda_1+1} - \frac{\rho_2\lambda_2}{\lambda_2-1}K_N^{-\lambda_2+1}\right.$$
$$\left.+\frac{\rho_2}{\lambda_2-1}K^{-\lambda_2+1} + K\right]. \quad \text{(A6)}$$

Combining (A1), (A3), and (A5) yields the call price function:

$$C(K;\mathbf{c},\boldsymbol{\theta}) = e^{-rT}[\sum_{i=1}^{n-5}c_i\int_K^{K_N}xB_{i,4}^{(1)}(x)\mathrm{d}x + \frac{\rho_1\lambda_1}{\lambda_1+1}K_1^{\lambda_1+1}$$
$$+\frac{\rho_2\lambda_2}{\lambda_2-1}K_N^{-\lambda_2+1} + \frac{\rho_1}{\lambda_1+1}K^{\lambda_1+1} - K]I_{[0,K_1)}(K)$$
$$+ e^{-rT}[\sum_{i=1}^{n-5}c_i(KB_{i,4}(K) + \int_K^{K_N}xB_{i,4}^{(1)}(x)\mathrm{d}x)$$
$$+\frac{\rho_2\lambda_2}{\lambda_2-1}K_N^{-\lambda_2+1} - K]I_{[K_1,K_N]}(K)$$
$$+ e^{-rT}\frac{\rho_2}{\lambda_2-1}K^{-\lambda_2+1}I_{(K_N,\infty]}(K).$$

Similarly, combining (A2), (A4), and (A6) yields the put price function:

$$P(K;\mathbf{c},\boldsymbol{\theta}) = e^{-rT}\frac{\rho_1}{\lambda_1+1}K^{\lambda_1+1}I_{[0,K_1)}(K)$$
$$+ e^{-rT}[\sum_{i=1}^{n-5}c_i(KB_{i,4}(K) - \int_{K_1}^K xB_{i,4}^{(1)}(x)\mathrm{d}x)$$
$$-\frac{\rho_1\lambda_1}{\lambda_1+1}K_1^{\lambda_1+1}]I_{[K_1,K_N]}(K) + e^{-rT}[-\sum_{i=1}^{n-5}c_iKB_{i,4}(K)$$
$$-\frac{\rho_1\lambda_1}{\lambda_1+1}K_1^{\lambda_1+1} - \frac{\rho_2\lambda_2}{\lambda_2-1}K_N^{-\lambda_2+1}$$
$$+\frac{\rho_2}{\lambda_2-1}K^{-\lambda_2+1} + K]I_{(K_N,\infty]}(K).$$

Appendix B: Derivation of the quadratic program

B.1. Loss function

$$\min_{\mathbf{c}\in\mathbb{R}^{n^*-5}} L_\omega = \sum_{i=1}^N(V(K_i) - V(K_i;\mathbf{c}\mid\boldsymbol{\theta}^*))^2 + w\int_{K_1}^{K_N}[R'''(x;\mathbf{c}\mid\boldsymbol{\theta}^*)]^2dx$$
$$= \epsilon^{\mathrm{T}}\epsilon + \omega\int_{K_1}^{K_N}[R'''(x;\mathbf{c}|\boldsymbol{\theta}^*)]^2\mathrm{d}x,$$

where

$$\epsilon = \mathbf{V} - \widehat{\mathbf{V}}|\boldsymbol{\theta}^*,$$

with

$$\mathbf{V} = \begin{bmatrix} V(K_1) \\ \\ \vdots \\ \\ V(K_N) \end{bmatrix} = \begin{bmatrix} P(K_1) \\ \vdots \\ P(K_p) \\ C(K_{p+1}) \\ \vdots \\ C(K_N) \end{bmatrix},$$

$$\widehat{\mathbf{V}}|\boldsymbol{\theta}^* = \begin{bmatrix} V(K_1;\mathbf{c}|\boldsymbol{\theta}^*) \\ \\ \vdots \\ \\ V(K_N;\mathbf{c}|\boldsymbol{\theta}^*) \end{bmatrix} = \begin{bmatrix} P(K_1;\mathbf{c}|\boldsymbol{\theta}^*) \\ \vdots \\ P(K_p;\mathbf{c}|\boldsymbol{\theta}^*) \\ C(K_{p+1};\mathbf{c}|\boldsymbol{\theta}^*) \\ \vdots \\ C(K_N;\mathbf{c}|\boldsymbol{\theta}^*) \end{bmatrix}.$$

B.1.1. Sum of squared errors (SSE)

Using the option price functions (21) and (22), we have

$$P(K_i;\mathbf{c}|\boldsymbol{\theta}^*) = e^{-rT}\left[\sum_{j=1}^{n-5} c_j(K_i B_{j,4}(K_i) - \int_{K_1}^{K} xB_{j,4}^{(1)}(x)dx) - \frac{\rho_1^*\lambda_1^*}{\lambda_1^*+1}K_1^{\lambda_1^*+1}\right],$$

$$C(K_i;\mathbf{c}|\boldsymbol{\theta}^*) = e^{-rT}\left[\sum_{j=1}^{n-5} c_j(K_i B_{j,4}(K_i) + \int_{K_i}^{K_N} xB_{j,4}^{(1)}(x)dx) + \frac{\rho_2^*\lambda_2^*}{\lambda_2^*-1}K_N^{-\lambda_2^*+1} - K_i\right],$$

whence

$$\widehat{\mathbf{V}}|\boldsymbol{\theta}^* = \begin{bmatrix} \mathbf{c}^{\mathrm{T}}\mathbf{M_1} - e^{-rT}\frac{\rho_1^*\lambda_1^*}{\lambda_1^*+1}K_1^{\lambda_1^*+1} \\ \vdots \\ \mathbf{c}^{\mathrm{T}}\mathbf{M_p} - e^{-rT}\frac{\rho_1^*\lambda_1^*}{\lambda_1^*+1}K_1^{\lambda_1^*+1} \\ \mathbf{c}^{\mathrm{T}}\mathbf{H_{p+1}} + e^{-rT}(\frac{\rho_2^*\lambda_2^*}{\lambda_2^*-1}K_N^{-\lambda_2^*+1} - K_{p+1}) \\ \vdots \\ \mathbf{c}^{\mathrm{T}}\mathbf{H_N} + e^{-rT}(\frac{\rho_2^*\lambda_2^*}{\lambda_2^*-1}K_N^{-\lambda_2^*+1} - K_N) \end{bmatrix},$$

where

$$\mathbf{M_i} = e^{-rT}\begin{bmatrix} K_iB_{1,4}(K_i) - \int_{K_1}^{K_i} xB_{1,4}^{(1)}(x)dx \\ \vdots \\ K_iB_{n-5,4}(K_i) - \int_{K_1}^{K_i} xB_{n-5,4}^{(1)}(x)dx \end{bmatrix},$$

$$\mathbf{H_i} = e^{-rT}\begin{bmatrix} K_iB_{1,4}(K_i) + \int_{K_i}^{K_N} xB_{1,4}^{(1)}(x)dx \\ \vdots \\ K_iB_{n-5,4}(K_i) + \int_{K_i}^{K_N} xB_{n-5,4}^{(1)}(x)dx \end{bmatrix}.$$

Let

$$\mathbf{W} = \begin{bmatrix} P(K_1) + e^{-rT}\frac{\rho_1^*\lambda_1^*}{\lambda_1^*+1}K_1^{\lambda_1^*+1} \\ \vdots \\ P(K_p) + e^{-rT}\frac{\rho_1^*\lambda_1^*}{\lambda_1^*+1}K_1^{\lambda_1^*+1} \\ C(K_{p+1}) - e^{-rT}(\frac{\rho_2^*\lambda_2^*}{\lambda_2^*-1}K_N^{-\lambda_2^*+1} - K_{p+1}) \\ \vdots \\ C(K_N) - e^{-rT}(\frac{\rho_2^*\lambda_2^*}{\lambda_2^*-1}K_N^{-\lambda_2^*+1} - K_N) \end{bmatrix},$$

$$\mathbf{G} = \begin{bmatrix} \mathbf{M_1^{\mathrm{T}}} \\ \vdots \\ \mathbf{M_p^{\mathrm{T}}} \\ \mathbf{H_{p+1}^{\mathrm{T}}} \\ \vdots \\ \mathbf{H_N^{\mathrm{T}}} \end{bmatrix},$$

then

$$\begin{aligned}\epsilon &= \mathbf{V} - \widehat{\mathbf{V}}|\boldsymbol{\theta}^* \\ &= \mathbf{W} - \mathbf{Gc},\end{aligned}$$

and

$$\begin{aligned}\epsilon^{\mathrm{T}}\epsilon &= (\mathbf{W} - \mathbf{Gc})^{\mathrm{T}}(\mathbf{W} - \mathbf{Gc}) \\ &= \mathbf{c}^{\mathrm{T}}\mathbf{G}^{\mathrm{T}}\mathbf{Gc} - 2\mathbf{W}^{\mathrm{T}}\mathbf{Gc} + \mathbf{W}^{\mathrm{T}}\mathbf{W}. \end{aligned} \quad \text{(B1)}$$

B.1.2. Roughness penalty

$$\begin{aligned}\int_{K_1}^{K_N}[R'''(x;\mathbf{c}\mid\boldsymbol{\theta}^*)]^2dx &= \int_{K_1}^{K_N}[\mathbf{c}^{\mathrm{T}}\mathbf{B^{(3)}}(x)]^2dx \\ &= \int_{K_1}^{K_N}\mathbf{c}^{\mathrm{T}}\mathbf{B^{(3)}}(x)\mathbf{B^{(3)}}(x)^{\mathrm{T}}\mathbf{c}\ dx, \end{aligned} \quad \text{(B2)}$$

where

$$\mathbf{B^{(3)}}(x) = \begin{bmatrix} B_{1,4}^{(3)}(x) \\ B_{2,4}^{(3)}(x) \\ \vdots \\ B_{n-6,4}^{(3)}(x) \\ B_{n-5,4}^{(3)}(x) \end{bmatrix}.$$

By construction, we have

$$\begin{aligned}\int_{x_i}^{x_{i+1}}\mathbf{c}^{\mathrm{T}}\mathbf{B^{(3)}}(x)\mathbf{B^{(3)}}(x)^{\mathrm{T}}\mathbf{c}\ dx &= h/3\frac{\gamma_{i+1}^3 - \gamma_i^3}{\gamma_{i+1} - \gamma_i} \\ &= \frac{h}{3}(\gamma_i^2 + \gamma_i\ \gamma_{i+1} + \gamma_{i+1}^2),\end{aligned}$$

where $\gamma_i = \mathbf{c}^{\mathrm{T}}\mathbf{B^{(3)}}(x_i)$, hence equation (B2) can be written in matrix form:

$$\begin{aligned}\int_{K_1}^{K_N}\mathbf{c}^{\mathrm{T}}\mathbf{B^{(3)}}(x)\mathbf{B^{(3)}}(x)^{\mathrm{T}}\mathbf{c}dx &= \sum_{i=5}^{n-5}\left[\int_{x_i}^{x_{i+1}}\mathbf{c}^{\mathrm{T}}\mathbf{B^{(3)}}(x)\mathbf{B^{(3)}}(x)^{\mathrm{T}}\mathbf{c}\ dx\right] \\ &= \sum_{i=5}^{n-5}\left[\frac{h}{3}(\gamma_i^2 + \gamma_i\gamma_{i+1} + \gamma_{i+1}^2)\right] \\ &= \mathbf{c}^{\mathrm{T}}\mathbf{D}^{\mathrm{T}}\mathbf{RDc}, \end{aligned} \quad \text{(B3)}$$

where

$$\mathbf{R} = \begin{bmatrix} \frac{h}{3} & \frac{h}{6} & 0 & 0 & \dots & 0 \\ \frac{h}{6} & \frac{2h}{3} & \frac{h}{6} & 0 & \dots & 0 \\ 0 & \frac{h}{6} & \ddots & \ddots & \ddots & \vdots \\ 0 & 0 & \ddots & \ddots & \frac{h}{6} & 0 \\ \vdots & \vdots & \ddots & \frac{h}{6} & \frac{2h}{3} & \frac{h}{6} \\ 0 & 0 & \dots & 0 & \frac{h}{6} & \frac{h}{3} \end{bmatrix},$$

$$\mathbf{D} = \begin{bmatrix} B_{1,4}^{(3)}(x_5) & \cdots & B_{n-5,4}^{(3)}(x_5) \\ \vdots & \vdots & \vdots \\ B_{1,4}^{(3)}(x_{n-4}) & \cdots & B_{n-5,4}^{(3)}(x_{n-4}) \end{bmatrix}.$$

By combining (B1) and (B3),

$$\min_{\mathbf{c}\in\mathbb{R}^{\mathbf{n}^*-\mathbf{5}}} L_\omega = \sum_{i=1}^{N} (V(K_i) - V(K_i;\mathbf{c} \mid \boldsymbol{\theta}^*))^2 + \omega \int_{K_1}^{K_N} [R'''(x;\mathbf{c} \mid \boldsymbol{\theta}^*)]^2 \mathrm{d}x$$

$$= \mathbf{c}^{\mathrm{T}}[\mathbf{G}^{\mathrm{T}}\mathbf{G} + \omega \mathbf{D}^{\mathrm{T}}\mathbf{R}\mathbf{D}]\mathbf{c} - 2\mathbf{W}^{\mathrm{T}}\mathbf{G}\mathbf{c} + \mathbf{W}^{\mathrm{T}}\mathbf{W}.$$

The optimization problem (27) is equivalent to the following quadratic program:

$$\min_{\mathbf{c}\in\mathbb{R}^{\mathbf{n}^*-\mathbf{5}}} L_\omega = \frac{1}{2}\mathbf{c}^{\top}\mathbf{Q}\mathbf{c} + \mathbf{F}\mathbf{c},$$

where

$$\mathbf{Q} = \mathbf{G}^{\top}\mathbf{G} + \omega \mathbf{D}^{\top}\mathbf{R}\mathbf{D},$$

$$\mathbf{F} = -\mathbf{W}^{\top}\mathbf{G}.$$

B.2. Constraints for the B-spline RNM CDF with power tails

B.2.1. End point conditions

By differentiating the B-spline basis function at knot points, the knot values of the B-spline basis function up to the second derivative are given by

$$B_{j,4}(x) = \begin{cases} \frac{1}{24} & x = x_{j+1}, \\ \frac{11}{24} & x = x_{j+2}, \\ \frac{11}{24} & x = x_{j+3}, \\ \frac{1}{24} & x = x_{j+4}, \end{cases} \tag{B4}$$

$$B_{j,4}^{(1)}(x) = \begin{cases} \frac{1}{6h} & x = x_{j+1}, \\ \frac{1}{2h} & x = x_{j+2}, \\ -\frac{1}{2h} & x = x_{j+3}, \\ -\frac{1}{6h} & x = x_{j+4}, \end{cases} \tag{B5}$$

$$B_{j,4}^{(2)}(x) = \begin{cases} \frac{1}{2h^2} & x = x_{j+1}, \\ -\frac{1}{2h^2} & x = x_{j+2}, \\ -\frac{1}{2h^2} & x = x_{j+3}, \\ \frac{1}{2h^2} & x = x_{j+4}. \end{cases} \tag{B6}$$

Using the knot values of B-spline basis (B4), (B5), and (B6), the RNM can be written as

$$\begin{aligned} R(x_j) &= \sum_{i=1}^{n-5} c_i B_{i,4}(x_j) \\ &= c_{j-4}B_{j-4,4}(x_j) + c_{j-3}B_{j-3,4}(x_j) + c_{j-2}B_{j-2,4}(x_j) \\ &\quad + c_{j-1}B_{j-1,4}(x_j) \\ &= \frac{c_{j-4} + 11c_{j-3} + 11c_{j-2} + c_{j-1}}{24}, \end{aligned} \tag{B7}$$

$$\begin{aligned} R'(x_j) &= \sum_{i=1}^{n-5} c_i B_{i,4}^{(1)}(x_j) \\ &= c_{j-4}B_{j-4,4}^{(1)}(x_j) + c_{j-3}B_{j-3,4}^{(1)}(x_j) + c_{j-2}B_{j-2,4}^{(1)}(x_j) \\ &\quad + c_{j-1}B_{j-1,4}^{(1)}(x_j) \\ &= \frac{-c_{j-4} - 3c_{j-3} + 3c_{j-2} + c_{j-1}}{6h}, \end{aligned} \tag{B8}$$

$$\begin{aligned} R''(x_j) &= \sum_{i=1}^{n-5} c_i B_{i,4}^{(2)}(x_j) \\ &= c_{j-4}B_{j-4,4}^{(2)}(x_j) + c_{j-3}B_{j-3,4}^{(2)}(x_j) + c_{j-2}B_{j-2,4}^{(2)}(x_j) \\ &\quad + c_{j-1}B_{j-1,4}^{(2)}(x_j) \\ &= \frac{c_{j-4} - c_{j-3} - c_{j-2} + c_{j-1}}{2h^2}. \end{aligned} \tag{B9}$$

With the knot values of RNM (B7), (B8), and (B9), the end point conditions (10)–(15) can be expressed as

$$\frac{c_1 + 11c_2 + 11c_3 + c_4}{24} = \rho_1^* K_1^{\lambda_1^*},$$

$$\frac{-c_1 - 3c_2 + 3c_3 + c_4}{6h} = \rho_1^* \lambda_1^* K_1^{\lambda_1^* - 1},$$

$$\frac{c_1 - c_2 - c_3 + c_4}{2h^2} = \rho_1^* \lambda_1^* (\lambda_1^* - 1) K_1^{\lambda_1^* - 2},$$

and

$$\frac{c_{n-8} + 11c_{n-7} + 11c_{n-6} + c_{n-5}}{24} = 1 - \rho_2^* K_N^{-\lambda_2^*},$$

$$\frac{-c_{n-8} - 3c_{n-7} + 3c_{n-6} + c_{n-5}}{6h} = \rho_2^* \lambda_2^* K_N^{-\lambda_2^* - 1},$$

$$\frac{c_{n-8} - c_{n-7} - c_{n-6} + c_{n-5}}{2h^2} = -\rho_2^* \lambda_2^* (\lambda_2^* + 1) K_N^{-\lambda_2^* - 2}.$$

The end point conditions (10)–(15) can then be written in matrix form:

$$\begin{bmatrix} 1 & 11 & 11 & 1 & 0 & \dots & 0 & 0 & 0 & 0 & 0 \\ -1 & -3 & 3 & 1 & 0 & \dots & 0 & 0 & 0 & 0 & 0 \\ 1 & -1 & -1 & 1 & 0 & \dots & 0 & 0 & 0 & 0 & 0 \\ 0 & 0 & 0 & 0 & 0 & \dots & 0 & 1 & 11 & 11 & 1 \\ 0 & 0 & 0 & 0 & 0 & \dots & 0 & -1 & -3 & 3 & 1 \\ 0 & 0 & 0 & 0 & 0 & \dots & 0 & 1 & -1 & -1 & 1 \end{bmatrix} \times \begin{bmatrix} c_1 \\ c_2 \\ \vdots \\ c_{n-6} \\ c_{n-5} \end{bmatrix} = \begin{bmatrix} 24\rho_1^* K_1^{\lambda_1^*} \\ 6h\rho_1^*\lambda_1^* K_1^{\lambda_1^*-1} \\ 2h^2\rho_1^*\lambda_1^*(\lambda_1^*-1)K_1^{\lambda_1^*-2} \\ 24(1-\rho_2^* K_N^{-\lambda_2^*}) \\ 6h\rho_2^*\lambda_2^* K_N^{-\lambda_2^*-1} \\ -2h^2\rho_2^*\lambda_2^*(\lambda_2^*+1)K_N^{-\lambda_2^*-2} \end{bmatrix}.$$

B.2.2. Non-negative probability condition

Using (C8), the non-negative probability condition (16) can be expressed as

$$\begin{aligned} R'(x_j) &= \sum_{i=1}^{n-5} c_i B_{i,4}^{(1)}(x_j) \\ &= c_{j-4}B_{j-4,4}^{(1)}(x_j) + c_{j-3}B_{j-3,4}^{(1)}(x_j) + c_{j-2}B_{j-2,4}^{(1)}(x_j) \\ &\quad + c_{j-1}B_{j-1,4}^{(1)}(x_j) \\ &= \frac{-c_{j-4} - 3c_{j-3} + 3c_{j-2} + c_{j-1}}{6h} \geq 0, \\ j &= 6, \dots, n-5. \end{aligned}$$

The non-negative probability condition (16) can then be written in matrix form:

$$\begin{bmatrix} 0 & -1 & -3 & 3 & 1 & 0 & 0 & 0 & \dots & 0 \\ 0 & 0 & -1 & -3 & 3 & 1 & 0 & 0 & \dots & 0 \\ \vdots & \vdots & & \ddots & \ddots & \ddots & \ddots & \vdots & \vdots & \vdots \\ 0 & \dots & 0 & 0 & -1 & -3 & 3 & 1 & 0 & 0 \\ 0 & \dots & 0 & 0 & 0 & -1 & -3 & 3 & 1 & 0 \end{bmatrix} \times \begin{bmatrix} c_1 \\ c_2 \\ \vdots \\ c_{n-6} \\ c_{n-5} \end{bmatrix} \geq \mathbf{0}.$$

B.2.3. Mean-forward price equality condition

The mean-forward price equality condition (20) is given by

$$\begin{aligned} S^0 e^{(r-d)T} &= \int_0^\infty x R'(x)\mathrm{d}x \\ &= \int_0^{K_1} \rho_1^*\lambda_1^* x^{\lambda_1^*} dx + \sum_{i=1}^{n-5} c_i \int_{K_1}^{K_N} x B_{i,4}^{(1)}(x)\ \mathrm{d}x \\ &\quad + \int_{K_N}^\infty \rho_2^*\lambda_2^* x^{-\lambda_2^*}\ dx \\ &= \frac{\rho_1^*\lambda_1^*}{\lambda_1^*+1}K_1^{\lambda_1^*+1} + \sum_{i=1}^{n-5} c_i \int_{K_1}^{K_N} x B_{i,4}^{(1)}(x)\mathrm{d}x \\ &\quad + \frac{\rho_2^*\lambda_2^*}{\lambda_2^*-1}K_N^{-\lambda_2^*+1} \end{aligned} \tag{B10}$$

Equation (B10) can then be written in matrix form:

$$\begin{bmatrix} \int_{K_1}^{K_N} x B_{1,4}^{(1)}(x)\mathrm{d}x \dots \int_{K_1}^{K_N} x B_{n-5,4}^{(1)}(x)\ \mathrm{d}x \end{bmatrix} \begin{bmatrix} c_1 \\ c_2 \\ \vdots \\ c_{n-6} \\ c_{n-5} \end{bmatrix}$$

$$= S_0 e^{(r-d)T} - \frac{\rho_1^*\lambda_1^*}{\lambda_1^*+1}K_1^{\lambda_1^*+1} - \frac{\rho_2^*\lambda_2^*}{\lambda_2^*-1}K_N^{-\lambda_2^*+1}.$$

Appendix C: Parametric distributions for the RNM

C.1. Log-normal distribution (LN)

The risk-neutral density function for $\log S_T$ is given by

$$q(z) = \frac{1}{\beta\sqrt{2\pi}}\, e^{-(z-\alpha)^2/2\beta^2},$$

where $z = \log S_T$ and S_T is the underlying asset price on the maturity date.

C.2. Log-stable distribution (LS)

The risk-neutral density function for $\log S_T$ is given by†

$$\begin{aligned} q(z) &= s(z_1;\alpha,-1,c_A T^{1/\alpha},\delta) * ts_+(z_2;\alpha,c_N T^{1/\alpha},0,1) \\ &= e^{\delta + c_N^\alpha \sec(\pi\alpha/2)T} s(z_1;\alpha,-1,c_A T^{1/\alpha},\delta) \\ &\quad * e^{-z_2} s(z_2;\alpha,+1,c_N T^{1/\alpha},0), \end{aligned} \tag{C1}$$

†The convolution of f and g is written as $f*g$. If X and Y are two independent random variables with probability distributions f and g, respectively, then the probability distribution of the sum $z = X + Y$ is given by the convolution

$$(f*g)(z) = \int f(\tau)g(z-\tau)d\tau$$

where $s(\cdot)$ is a stable density function, and $ts_+(\cdot)$ is an exponentially tilted positively skewed stable density.

Under the risk-neutral density (C1), the characteristic function of the log price $z \equiv \log S_T$ is given by

$$cf_q(u) = \exp\Big[iu\Big(\log S_0 + (r-d)T - (c_N^{\alpha} - c_A^{\alpha})\sec\Big(\frac{\pi\alpha}{2}\Big)T\Big)$$

$$-c_A{}^{\alpha}\sec\Big(\frac{\pi\alpha}{2}\Big)(iu)^{\alpha}T + c_N{}^{\alpha}\sec\Big(\frac{\pi\alpha}{2}\Big)(1-(1-iu)^{\alpha})T\Big].$$

C.3. Double log-normal distribution (DN)

The risk-neutral density function for $\log S_T$ is given by

$$q(z) = \omega\phi(z;\alpha_1,\beta_1) + (1-\omega)\phi(z;\alpha_2,\beta_2)$$

$$= \omega\frac{1}{\beta_1\sqrt{2\pi}}e^{-(z-\alpha_1)^2/2\beta_1^2} + (1-\omega)\frac{1}{\beta_2\sqrt{2\pi}}e^{-(z-\alpha_2)^2/2\beta_2^2},$$

where $\beta_j = \sigma_j\sqrt{T}$ and $\phi(\cdot)$ is a normal density function.

C.4. Double log-stable distribution (DS)

The risk-neutral density function for $\log S_T$ is given by

$$\begin{aligned} q(z) &= \omega s(z;\alpha_1,-1,c_1T^{1/\alpha_1},\delta_1) \\ &\quad + (1-\omega)ts_+(z;\alpha_2,c_2T^{1/\alpha_2},\delta_2,1) \\ &= \omega s(z;\alpha_1,-1,c_1T^{1/\alpha_1},\delta_1) \\ &\quad + (1-\omega)e^{\delta_2 + c_2^{\alpha_2}T\sec(\pi\alpha_2/2)}e^{-z}s(z;\alpha_2,1,c_2T^{1/\alpha_2},\delta_2), \end{aligned} \tag{C2}$$

where $s(\cdot)$ is a stable density function, and $ts_+(\cdot)$ is an exponentially tilted positively skewed stable density.Under the risk-neutral density (C2), the characteristic function of the log price $z \equiv \log S_T$ is given by

$$cf_q(u) = \omega cf_{q_1}(u) + (1-\omega)cf_{q_1}(u)$$

$$= \omega e^{iu\delta_1 - c_1{}^{\alpha_1}\sec(\pi\alpha_1/2)(iu)^{\alpha_1}T} + (1 - \omega)e^{iu\delta_2 + c_2{}^{\alpha_2}\sec(\pi\alpha_2/2)(1-(1-iu)^{\alpha_2})T}.$$

C.5. Generalized log-stable distribution (GS)

The risk-neutral density function for $\log S_T$ is given by

$$q(z) = *_{j=1}^{2} ts(z_j;\alpha,\mathrm{sgn}(c_{Nj}-c_{Aj}),\mid c_{Nj}-c_{Aj}\mid T^{1/\alpha},\delta_j,\Big|\frac{c_{Nj}}{c_{Nj}-c_{Aj}}\Big|), \tag{C3}$$

where $ts(\cdot)$ is an exponentially tilted positively skewed stable density if $\mathrm{sgn}(c_{Nj}-c_{Aj}) = 1$ or an exponentially tilted negatively skewed stable density if $\mathrm{sgn}(c_{Nj}-c_{Aj}) = -1$ and $*$ denotes the convolution operator.Under the risk-neutral density (C3), the characteristic function of the log price $z \equiv \log S_T$ is given by

$$cf_q(u) = \exp\Big\{iu\Big(\log S_0 + (r-d)T - \sum_{j=1}^{2}(c_{Nj}{}^{\alpha} - c_{Aj}{}^{\alpha})\sec\big(\tfrac{\pi\alpha}{2}\big)T\Big) + \sum_{j=1}^{2}|c_{Nj}-c_{Aj}|^{\alpha}\sec\big(\tfrac{\pi\alpha}{2}\big) \cdot\Big[\Big|\frac{c_{Nj}}{c_{Nj}-c_{Aj}}\Big|^{\alpha} - \Big(\Big|\frac{c_{Nj}}{c_{Nj}-c_{Aj}}\Big| - \mathrm{sgn}(c_{Nj}-c_{Aj})iu\Big)^{\alpha}\Big]T\Big\}.$$

C.6. Weibull distribution (WB)

The risk-neutral density function for S_T is given by

$$r(x) = \begin{cases} \big(\frac{\beta}{\alpha}\big)\big(\frac{x}{\alpha}\big)^{\beta-1}e^{-(x/\alpha)^{\beta}}, & \text{for all } x \geq 0, \\ 0, & \text{for all } x<0. \end{cases}$$

C.7. Generalized gamma distribution (GG)

The risk-neutral density function for S_T is given by

$$r(x) = \begin{cases} \frac{1}{\Gamma(p)}\big(\frac{|\beta|}{\alpha}\big)\big(\frac{x}{\alpha}\big)^{\beta p-1}e^{-(x/\alpha)^{\beta}}, & \text{for all } \mathrm{x} \geq 0, \\ 0, & \text{for all } \mathrm{x}<0, \end{cases}$$

where

$$\Gamma(p) = \int_0^{\infty} u^{p-1}e^{-u}\mathrm{d}u \quad \text{(Gamma function)}.$$

C.8. Generalized beta distribution (GB)

The risk-neutral density function for S_T is given by

$$r(x) = \begin{cases} \frac{|\beta|x^{\beta p-1}}{\alpha^{\beta p}B(p,q)[1+(x/\alpha)^{\beta}]^{p+q}}, & \text{for all } x \geq 0, \\ 0, & \text{for all } x<0, \end{cases}$$

where

$$B(p,q) = \frac{\Gamma(p)\Gamma(q)}{\Gamma(p+q)} = \int_0^{\infty}\frac{u^{p-1}}{(1+u)^{p+q}}\mathrm{d}u \quad \text{(Beta function)}$$

$$= \int_0^1 w^{p-1}(1-w)^{q-1}\mathrm{d}w, \quad w = \frac{1}{u+1}.$$

C.9. Fixed moment log-stable distribution (FS)

The risk-neutral density function for $\log S_T$ is given by

$$q(z) = s(z;\alpha,-1,c\ T^{1/\alpha},\delta), \tag{C4}$$

where $s(\cdot)$ is the stable density function.

Under the risk-neutral density (C4), the characteristic function of the log price $z \equiv \log S_T$ is given by

$$cf_q(u) = \exp[iu(\log S_0 + (r-d)T + c^\alpha \sec\left(\frac{\pi\alpha}{2}\right)T) - c^\alpha \sec\left(\frac{\pi\alpha}{2}\right)(iu)^\alpha T].$$

C.10. Variance-Gamma distribution (VG)

The risk-neutral density function for $\log S_T$ is given by

$$q(z) = \int_0^\infty \frac{1}{\sigma\sqrt{2\pi g}} e^{-[(z-\log S_0-(r-d+\mu)T-\beta g)^2]/2\sigma^2 g} \frac{g^{t/\alpha-1} e^{-g/\alpha}}{\alpha^{t/\nu}\Gamma(t/\alpha)} \mathrm{d}g, \tag{C5}$$

where $g = \gamma(t+h;\mu,\alpha) - \gamma(t;\mu,\alpha)$ and $\gamma(\cdot;\mu,\alpha)$ is a gamma process. The additional two parameters α and β relative to the geometric Brownian motion control the skewness and kurtosis, respectively. Under the risk-neutral density (C5), the characteristic function of the log price $z \equiv \log S_T$ is given by

$$cf_q(u) = e^{iu(\log S_0+(r-d+\mu)T)}[1 - (i\beta u - \frac{1}{2}\sigma^2 u^2)\alpha]^{-T/\alpha}.$$

C.11. Poisson jump diffusion process (JD)

The risk-neutral process for S_t is

$$\frac{\mathrm{d}S_t}{S_t} = ((r-d) - \lambda\mu_J)\mathrm{d}t + \sigma \mathrm{d}W_t^s + J_t \mathrm{d}q_t, \tag{C6}$$

where W_t^s is a standard Brownian motion, $J(t)$ is the percentage jump size (conditional on no jump occurring) with $\log(1+J_t) \sim N(\log(1+\mu_J) - 1/2\sigma_J^2, \sigma_J^2)$, and $q(t)$ is a Poisson jump counter with intensity λ, i.e. $\Pr[\mathrm{d}q(t)=1] = \lambda \mathrm{d}t$, $\Pr[\mathrm{d}q(t)=0] = 1-\lambda \mathrm{d}t$. Under the risk-neutral process (C6), the characteristic function of the log price $z \equiv \log S_T$ is given by

$$cf_q(u) = \exp\left[iu(\log S_0 + (r-d)T - \lambda\mu_J T - \frac{1}{2}\sigma^2) - \frac{1}{2}u^2\sigma^2 T + \lambda(e^{iu(\log(1+\mu_J)-1/2\sigma_J^2)-1/2u^2\sigma_J^2} - 1)T\right].$$

C.12. Jump diffusion process with stochastic volatilities (JS)

The risk-neutral process for S_t is given by

$$\frac{\mathrm{d}S_t}{S_t} = ((r-d) - \lambda\mu_J)\mathrm{d}t + \sqrt{V_t}\ \mathrm{d}W_t^s + J_t\ \mathrm{d}q_t, \tag{C7}$$

$$\mathrm{d}V_t = \kappa(\vartheta - V_t)\ \mathrm{d}t + \sigma_v\sqrt{V_t}\ \mathrm{d}W_t^v, \tag{C8}$$

where V_t is the diffusion component of the return variance (conditional on no jump occurring),† W_t^s and W_t^v are a standard Brownian motion, respectively, with $\mathrm{Cov}_t[dW_t^s, dW_t^v] = \rho\ \mathrm{d}t$, $J(t)$ is the percentage jump size (conditional on no jump occurring) with $\log(1+J_t) \sim N(\log(1+\mu_J) - 1/2\sigma_J^2, \sigma_J^2)$, $q(t)$ is a Poisson jump counter with intensity λ, and κ, ϑ, and σ_v are, respectively, the speed of adjustment, the long-run mean and the variation coefficient of the diffusion volatility V_t.

Under the risk-neutral process (C7) and (C8), the characteristic function of the log price $z \equiv \log S_T$ is given by

$$cf_q(u) = \exp\Big\{iu(\log S_0 + (r-d)T - \lambda\mu_J T) + \lambda[e^{iu(\log(1+\mu_J)-1/2\sigma_J^2)-1/2u^2\sigma_J^2} - 1]T - C(u)V_t - D(u)\Big\},$$

where

$$C(u) = \frac{\xi(1-e^{-\eta T})}{2\eta - (\eta-\kappa^*)(1-e^{-\eta T})},$$

$$D(u) = \frac{\kappa\vartheta}{\sigma_v^2}\left[2\log\left(1 - \frac{(\eta-\kappa^*)(1-e^{-\eta T})}{2\eta}\right) + (\eta-\kappa^*)T\right],$$

$$\eta = \sqrt{(\kappa^*)^2 + \sigma_v^2\xi},$$

$$\kappa^* = \kappa - iu\sigma_v\rho,$$

$$\xi = iu + u^2.$$

†The current level of V_t is unobservable. Thus, the state variable V_t is essentially treated as another free parameter in the RNM estimation procedure (Carr and Wu 2003).